AD-A131 363 IN-SITU LIGHT SCATTERING TECHNIQUES FOR DETERMINING 1/1
AEROSOL SIZE DISTRIBU..(U) GEORGIA INST OF TECH ATLANTA
SCHOOL OF GEOPHYSICAL SCIENCES G W GRAMS 29 JUN 83
UNCLASSIFIED ARO-16462.1-GS DAAG29-79-C-0092 F/G 20/6 NL

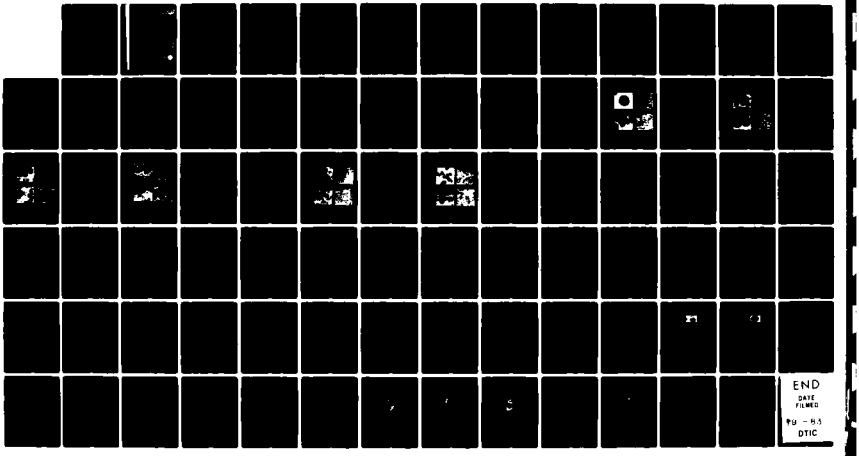

END
DATE FILMED
9 - 83
DTIC

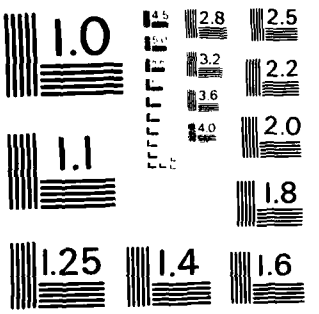

MICROCOPY RESOLUTION TEST CHART
NATIONAL BUREAU OF STANDARDS - 1963 - A

ARO 16462.1-GS

AD A131363

FINAL REPORT

IN-SITU LIGHT SCATTERING TECHNIQUES FOR DETERMINING AEROSOL SIZE DISTRIBUTIONS AND OPTICAL CONSTANTS

By

Gerald W. Grams

June 1983

Prepared for

U.S. ARMY RESEARCH OFFICE

Under

Contract Number DAAG29-79-C-0092

DTIC
ELECTE
AUG 16 1983
D

GEORGIA INSTITUTE OF TECHNOLOGY
A UNIT OF THE UNIVERSITY SYSTEM OF GEORGIA
SCHOOL OF GEOPHYSICAL SCIENCES
ATLANTA, GEORGIA 30332

DTIC FILE COPY

83 08 15 029

APPROVED FOR PUBLIC RELEASE;
DISTRIBUTION UNLIMITED

IN-SITU LIGHT SCATTERING TECHNIQUES FOR DETERMINING AEROSOL SIZE DISTRIBUTIONS AND OPTICAL CONSTANTS

FINAL REPORT

GERALD W. GRAMS

JUNE 29, 1983

U.S. ARMY RESEARCH OFFICE

CONTRACT NUMBER DAAG29-79-C-0092

SCHOOL OF GEOPHYSICAL SCIENCES
GEORGIA INSTITUTE OF TECHNOLOGY
ATLANTA, GEORGIA 30332

APPROVED FOR PUBLIC RELEASE;
DISTRIBUTION UNLIMITED.

Accession For
NTIS GRA&I
DTIC TAB
Unannounced
Justification
By
Distribution/
Availability Codes
Dist | Avail and/or Special
A

THE VIEW, OPINIONS, AND/OR FINDINGS CONTAINED IN THIS REPORT ARE THOSE OF THE AUTHOR(S) AND SHOULD NOT BE CONSTRUED AS AN OFFICIAL DEPARTMENT OF THE ARMY POSITION, POLICY, OR DECISION, UNLESS SO DESIGNATED BY OTHER DOCUMENTATION.

SECURITY CLASSIFICATION OF THIS PAGE (When Data Entered)

REPORT DOCUMENTATION PAGE	READ INSTRUCTIONS BEFORE COMPLETING FORM
1. REPORT NUMBER	2. GOVT ACCESSION NO. AD-A128363	3. RECIPIENT'S CATALOG NUMBER
4. TITLE (and Subtitle) In-situ Light Scattering Techniques for Determining Aerosol Size Distributions and Optical Constants	5. TYPE OF REPORT & PERIOD COVERED Final 1 May 1974 - 30 April 1983 6. PERFORMING ORG. REPORT NUMBER
7. AUTHOR(s) Gerald W. Grams	8. CONTRACT OR GRANT NUMBER(s) DAAG29-79-C-0092
9. PERFORMING ORGANIZATION NAME AND ADDRESS School of Geophysical Sciences Georgia Institute of Technology Atlanta, Georgia 30332	10. PROGRAM ELEMENT, PROJECT, TASK AREA & WORK UNIT NUMBERS Project #P-16462-GS
11. CONTROLLING OFFICE NAME AND ADDRESS U. S. Army Research Office Post Office Box [illegible] Research Triangle Park, [illegible] 27709	12. REPORT DATE June 29, 1983 13. NUMBER OF PAGES 78
14. MONITORING AGENCY NAME & ADDRESS(if different from Controlling Office)	15. SECURITY CLASS. (of this report) Unclassified 15a. DECLASSIFICATION/DOWNGRADING SCHEDULE

16. DISTRIBUTION STATEMENT (of this Report)

Approved for public release; distribution unlimited.

17. DISTRIBUTION STATEMENT (of the abstract entered in Block 20, if different from Report)

N/A

18. SUPPLEMENTARY NOTES

THE VIEW, OPINIONS, AND/OR FINDINGS CONTAINED IN THIS REPORT ARE THOSE OF THE AUTHOR(S) AND SHOULD NOT BE CONSTRUED AS AN OFFICIAL DEPARTMENT OF THE ARMY POSITION, POLICY, OR DECISION, UNLESS SO DESIGNATED BY OTHER DOCUMENTATION.

19. KEY WORDS (Continue on reverse side if necessary and identify by block number)

Light scattering, aerosol particles, laser measurements, optical constants

20. ABSTRACT (Continue on reverse side if necessary and identify by block number)

The research performed under this program has focused on studying optical properties of non-spherical particles in the laboratory. It required the development of techniques for routinely generating and collecting artificial aerosols of known chemical composition, for performing light scattering measurements, and for interpreting light scattering data. Progress on each technique has been achieved, and the principal results for each of these three basic activities are discussed in this report.

DD FORM 1 JAN 73 1473 EDITION OF 1 NOV 65 IS OBSOLETE

SECURITY CLASSIFICATION OF THIS PAGE (When Data Entered)

TABLE OF CONTENTS

INTRODUCTION

The research performed under this program has focused on studying optical properties of non-spherical particles in the laboratory. It required the development of techniques for routinely generating and collecting artificial aerosols of known chemical composition, for performing light scattering measurements, and for interpreting light scattering data. Progress on each techniuqe has been achieved and we will discuss the main results for each of these three basic activities separately. Along with the results, we shall also discuss our conclusions and recommendations for future research.

1. Generation and Collection of Optical Aerosols

1.1 Experimental Techniques

We used two different kinds of generators for our studies - one for monodisperse aerosols and one for polydisperse aerosols:

a) The monodisperse aerosol generator was a TSI Model 3050, a commercially available instrument that operates with an ultrasonic vibrator that breaks a liquid jet into equal-volume droplets. The liquid in the jet is a solution of known chemicals and, after the droplets dry out in a flow of clean air, they leave residual particles with characteristic shapes. Some examples of the types of particles obtained with this device are shown in Appendix I.

b) The polydisperse aerosol generator was assembled in our laboratory as a reproduction of one of the aerosol generators used during the First Workshop on Light Absorbing Particles, Fort Collins, Colorado, in 1980 (Gerber and Hindman, 1982). Compressed air flows through each of three bottles in series. Each bottle is partially filled with the solution used to form the particles. Air passing through the first bottle becomes saturated with respect to the chemical solution being used to

generate the particles. If saturated air from the first bottle is bubbled through the liquid in the second bottle, the concentration of that liquid will not change since evaporation losses will be minimized. The bubbles in bottle #2 break and cause droplets to be injected into the air. A jet of air with suspended droplets from the second bottle is directed toward the surface of the liquid in the third bottle so that the largest of the droplets will be removed by impaction. The smaller droplets proceed through the system, they evaporate in dry air, and the droplet residue then forms a polydisperse aerosol. This system was simple to assemble, operated steadily for long periods of time, and generated reproducible aerosol size distributions from one experiment to another.

For aerosol collection we used nuclepore filters made of polycarbonate membrane with hole diameters of 0.4 μm. Circular filters with diameters of 25 mm were used for short sampling times of the order of 10 min, and filters with diameters of 47 mm were used for long sampling times of the order of a few hours. In both cases we used plastic filter holders and a sampling differential pressure of 25 cm Hg. The shorter aerosol sampling times were used for the filters to be analyzed with the scanning electron microscope; in that case the aerosol flow was sampled through a 1-mm hole in the cap of the filter holder. The long filtration times were used for determination of the mass by weight; for those cases, no caps were used during the filtration process.

1.2 Results

A monodisperse aerosol generator (TSI Model 3050) was used for generating the non-spherical, non-homogeneous aerosol particles during our light scattering study. The vibrating orifice generator is capable of producing a continuous flow of practically monodisperse droplets of known chemical solutions. In our experimental

apparatus the droplets were rapidly evaporated in a relatively strong flow of filtered dry air ($\sim$ 6 m^3/hour) and samples of the remaining dry residue were collected on nuclepore filters after passing through a 1-m length of 46-mm diameter metallic tubing which served as an aerosol flow tube for the Georgia Tech laser polar nephelometer (Grams et al., 1975). Figure 1 shows schematically the experimental set-up along with some additional technical information.

Analyses of the filters with a scanning electron microscope (SEM) enabled us to determine morphological characteristics of the particles such as the particle shape and size as well as the roughness and degree of irregularity of the surfaces. It also allowed us to establish the amount of uniformity amongst the monodisperse particles. Examples of the variety of particle characteristics obtained with our aerosol generation system are shown in Appendix I.

All the chemical compounds used in our study were dissolved in a 50-50 solution of ethanol and water and loaded in a 50 cm^3 disposable plastic syringe. With the 20-μm diameter generator orifice and the gear ratio specified by the instruction manual of the aerosol generator, it proved to be straightforward to obtain continuous aerosol flows for time periods lasting from approximately two hours to a maximum of about six hours. No modifications were performed on the instrument, and the instrument was operated in accordance with the procedures outlined in the manufacturer's instruction manual.

The range of concentrations of the various compounds in the 50-50 ethanol-water solutions was between 6.6×10^{-6} to 6.3×10^{-3} (by volume) corresponding to particle sizes that were approximately between 1 and 6 μm (with the 20-μm generator orifice). While using a given compound, it was fairly easy to produce particles with a shape similar to those wanted; however, it proved to be difficult with our standard set-up to reproduce particles of the same size (within the uncertainties of the SEM) in different experiments. The compounds tested, and examples of the

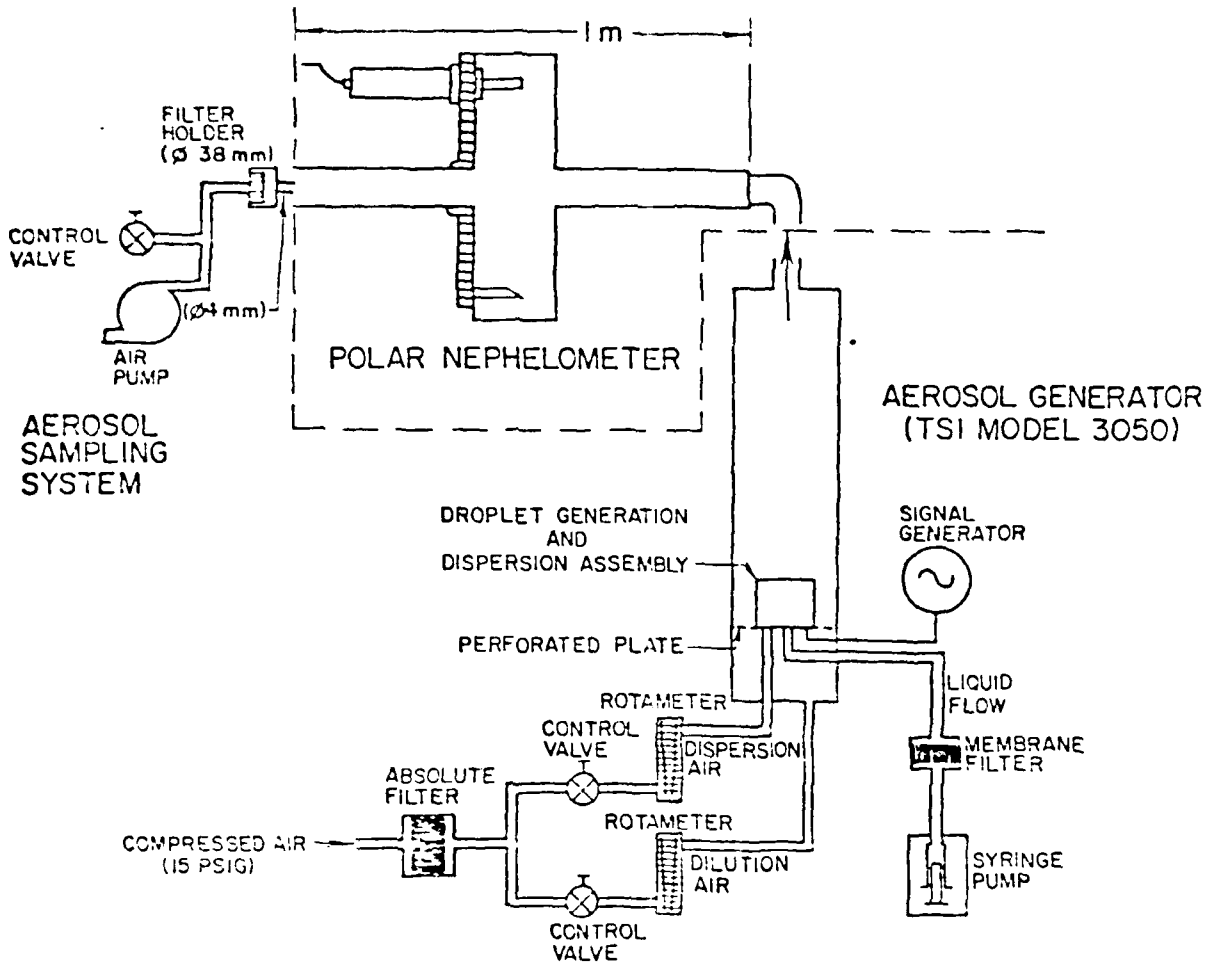

Figure 1. The experimental setup used in the measurements consisted of the Berglund-Liu generator, the Georgia Tech polar nephelometer and the system for Nuclepore filter aerosol sampling.

particles obtained in our laboratory are listed on the following pages along with other supplementary information. In addition to the material presented in the manufacturer's instruction manuals, additional examples and details on the vibrating orifice generator may be found in a variety of articles such as Berglund and Liu (1973), Pinnick et al. (1976), and Liu (1975).

It should be noted that our monodisperse particle generator was operated without the use of an option offered by the manufacturer, namely, a radiation source to prevent electrostatically charged particles. We regarded this attachment as an item that would be important for preventing the loss of aerosol particles to the walls of small diameter aerosol flow systems. Such losses are expected to increase with particle size and, for the range of particle sizes in our experiments, these losses were expected to be negligible. While our data supports such assumptions, we did encounter one effect that might have been eliminated by the use of the radiation source. In some of our filter samples, the SEM photographs showed particles that appeared to stick to each other as in Figure 4b of Appendix I. We believe that the fragile structures indicated in such photographs are formed by electrostatic attraction between individual particles on the filter surface (rather than in the air). For future work, we would recommend that the radiation source be used to prevent such effects and to provide better documentation on the morphology of the artificially generated particles.

The examples shown in Appendix I demonstrate that fairly good results can be obtained with the Berglund-Liu generator by simply following the instruction manual and without special instrumentation training. Our results to date indicate the most interesting particle shapes that we can generate are those that were obtained from mixtures of different compounds of known refractive indices as in Figure 6 of Appendix I. We hope in the near future to be able to extend these experiments with the aerosol generator to develop procedures for obtaining reproducible results for

a variety of unusual particle shapes.

On one hand, the development of ad hoc laboratory techniques is necessary for one to generate these unusual shapes. On the other hand, these particles are representative of the kind of particles actually occuring in nature and the shapes are of interest in many atmospheric applications. In fact, the particles that we generated by mixing 75% ammonium sulfate and 25% nigrosine dye in a 50-50 ethanol-water solution with a concentration of 6.6×10^{-7} by volume were similar to those measured by the NASA Langley Research Center with a quartz crystal microbalance in the stratosphere after the eruption of El Chichon volcano (Personal communication, David Woods, NASA/LaRC, 1982).

With regard to our "home made" system for generating a polydisperse aerosol, a "typical" size distribution obtained with the system is shown in Figure 2 for the case of a solution of sodium chloride. These measurements were obtained with a Knollenberg counter (PMS Model LAS-X). The aerosol polydispersions generated with this system did not appear to be electrostatically charged; the size distribution in these cases seemed to depend mostly on the surface tension of the solution and on the air pressure used for the bubbler during the experiments.

The main population of the particles from the polydisperse generator was usually in the size range around 0.1 micrometer radius. With water solutions at different concentrations, it was easy to change the mean size of the main population of the particles by a factor of two from this typical value. The generation of larger particle sizes could be achieved by replacing the capillary glass tubing in the second bottle with a porous glass pipette and drying the aerosol immediately after the particles left the second bottle. We ran only a few tests with the source in this configuration, and we did not measure its stability with time.

As the general conclusions of this section, we can make the following statements:

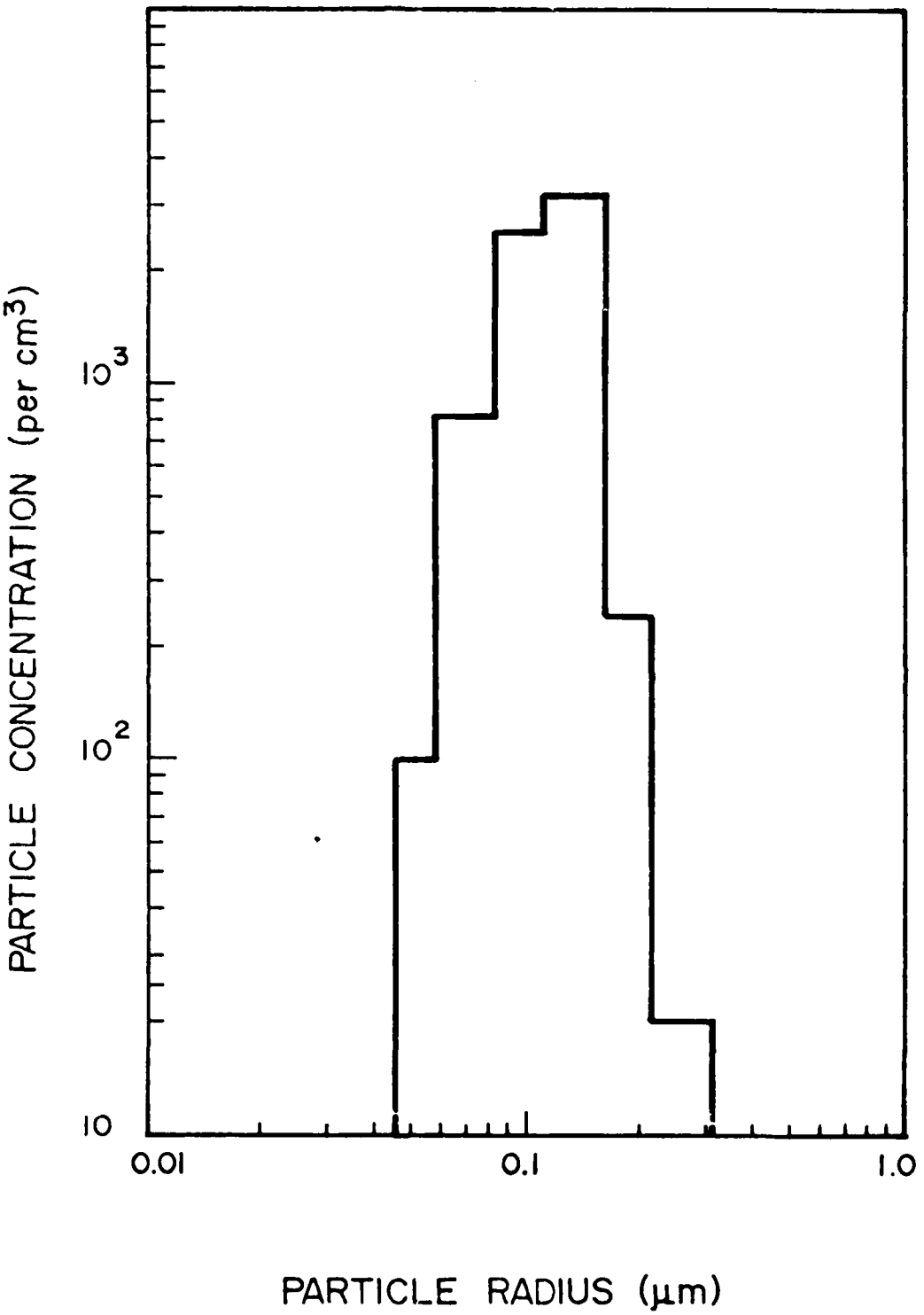

Figure 2. Typical size distribution for sodium chloride particles from the polydisperse aerosol generator.

- The Berglund Liu vibrating orifice generator proved to be a stable and dependable monodisperse aerosol source. The use of an orifice diameter of 20 μm permitted long and stable operation for particles in the size range between 0.5 μm and 2 μm radius with flow rates of the order of 10 particles/cm^2/s. The radiative source for neutralizing the particles is necessary only if there are specific reasons for sampling the aerosol with smaller diameter plastic tubing at low flow rates or for generating particle sizes larger than a few microns.
- Particle collection on filters for analyzing the particles at the SEM is straightforward and can be done with characteristic times of the order of 10 minutes. No particular care is needed unless it is necessary to avoid particle aggregation due to electrostatic charge or particle breaking due to the fragile nature of the particles (see Fig. 4b, Appendix I).
- Stable aerosol polydispersions in the submicron size range could be generated by bubbling air through solutions in the way that was described above; the stability of such sources is good and fairly well reproducible. The particle concentration depends mainly on the amount of diluting air used for drying the particles. If simple rubber stoppers are used on the bottles to maintain air pressure, typical maximum pressures are of the order of 14×10^3 Pa.

2. Light Scattering Measurements

2.1 Experimental Techniques and Results

A systematic description of the experimental apparatus and of the results are described in the attached Appendix II. Most of the data had been taken using a HeNe laser as a light source at 6328 Å for a polar nephelometer measuring scatter-

ing angles between 10 and 170° in two orthogonal planes of polarization of the incident light. An informal collection of most of the 90 measurements made during the course of our study is available upon request; the typical relative error on single data points was less than 10%. Other available light sources such as the dye laser. were not stable enough to perform dependable measurements.

2.2 Conclusions

From the viewpoint of the optical measurements, many interesting conclusions can be drawn. The polar nephelometer properly performed measurements of light scattering on the set of particles; we did not have any indication that the particles were not randomly oriented. This factor allowed us to rapidly measure the light scattering characteristics of particles without having to perform averaging on different orientations.

The only systematic uncertainty on the data set has been introduced by the percentage (typically less than 10%) of particles with double volume, generated along with the main population of monodisperse particles. Generally speaking, we noted that the following properties of monodisperse particles can be observed directly on the raw data prior to any specific data analysis; if the particles have a quasi-spherical symmetry with various irregular features appearing on their surfaces, it is possible to evaluate the size parameter x of the particles ($x = 2\pi r/\lambda$, where r is the radius and λ the wavelength of the illuminating beam) from the value of the angle θ_1 where the first observable diffraction minimum occurs in the scattering curve in coincidence with the first zero of the Bessel function of the first kind. This can be compared using the formula:

$$x = 3.83/\sin\theta_1$$

or, with less precision, from the angle θ_2 corresponding to the second minimum of the diffraction curve using the formula:

$$x = 7/\sin\theta_2 \ .$$

These results are almost independent of the shape and size of the particles. It is also possible to qualitatively estimate when a particle is light absorbing from the difference existing in the scattering intensities around 60° for two orthogonal planes of the polarized incident light; in fact, high values of polarization along this scattering direction can usually be associated with a high fraction of light absorbed inside the particles. While generally true, this rule cannot be applied to metallic particles or for particles with size parameters less than about 5.

3. Analysis of Light Scattering Data

3.1 Summary of Numerical Procedures

The final results of each experiment, after reducing the data for the gaseous scattering and instrumental response and averaging the various angular scans, consisted of graphs of the average measured intensities plotted versus angle in the interval 10-170° for each plane of polarization of the laser beam illuminating the flow of particles. We concentrated our attention on studying the characteristics of the normalized phase functions, $P_1(\theta)$ and $P_2(\theta)$, as defined by Diermendjian (1969), because these functions are independent of the number of particles per unit time crossing the laser beam or of any absolute calibration of the instrument. In fact, we measured particles for the interval of size parameters from $x = 5$ up to the value of $x = 30$, where the scattering cross section of the absorbing particle

is close to the value predicted by geometric optics. The asymmetry parameter,

$$g = \tfrac{1}{2} \int_{-1}^{1} \frac{P_1(\mu) + P_2(\mu)}{2} \mu \, d\mu \quad ,$$

where

$$\mu = \cos\theta \ ,$$

can be computed from the normalized data. For nonabsorbing particles, g is approximately related to the scattering efficiency factor by the relation:

$$Q_{sca} \ (1 - g) \simeq \text{constant}$$

for size parameters larger than 10. In both cases, it is possible to recover some of the information on scattering and extinction coefficients that have been lost in the normalization procedure.

Previous comparisons between the Mie theory and measurements taken with microwave and light scattering techniques gave apparently opposite results (Zerull, 1976; Pinnick et al., 1976). Therefore, it was rather important to choose a data analysis procedure that would lead to results as independent as possible from the specific experimental procedure. The numerical techniques used to normalize the data, to estimate the size parameter and to compute the asymmetry parameters, have been described in detail in Appendix II and will not be repeated here.

On all the data sets, we ran

- intercomparisons with the Mie theory for spherical particles;
- inversion procedures based on the Mie theory (Baker and Coletti, 1982)
- a modified version of the Pollack and Cuzzi (1980) theory;

- a least-squares inversion for determining the percentage of diffracted, reflected and refracted light from the scattering particles.

3.2 Conclusions

Non-light absorbing particles had measured phase functions that were almost featureless with only a few oscillations in the forward scattering and the backward scattering directions. Interestingly, the intercomparisons with the Mie theory for spherical particles showed that, in the cases where it was possible, the phase function best fitting the forward scattering did not fit as well in the backward scattering and vice versa. Somewhat analogous conclusions had been reached by Pinnick et al. (1976) who interpreted their data in terms of Mie spheres with concentric voids.

Our inversion program based on the Mie theory did not give definitive numerical results, and any expectations about representing measured light scattering with a set of "equivalent spheres" should not be encouraged at this point. For the non-spherical particles, we were not able to find any systematic relationships between the sizes of the particles measured and the retrieved sizes. The retrievals, in fact, appeared to be more dependent on our choice of size bins and error smoothing methods than on any of the obvious physical parameters for describing the irregular particles.

We did not have a great deal of success in applying the Pollack and Cuzzi (1980) theory for aerosol particle polydispersions to our monodisperse systems. This theory is, crudely speaking, based on describing the scattering pahse functions with the Mie theory for smaller particle sizes and letting the rest of the scattering contributions be represented by a combination of diffraction, reflection and transmission properties of the larger particles. In practice, the Mie curves that represented the best compromise for fitting the oscillations observed in the experi-

mental data in the forward and backward directions was such as to dramatically decrease the diffraction contributions by forcing the coefficients of reflected and refracted components toward unreasonable values compared with diffraction. On the other hand, if the Mie contributions were decreased, the resulting fits were unacceptable, because the reflected and refracted component were represented by functions that are somewhat similar to each other and could not be uniquely distinguished. A procedure of fitting the main forward scattering peak to diffraction patterns was, some of the time, in disagreement with the secondary peaks. Therefore, the forward scattering could not be properly represented by simple linear combinations of diffraction, transmission and reflection. Consequently, we devised our own non-linear procedure, as described in Appendix II, for the representation of the aerosol scattering patterns.

PARTICIPATING SCIENTIFIC PERSONNEL

Principal Investigator:

Gerald W. Grams

Professional Personnel:

Edward M. Patterson (Research Scientist)
Alessandro Coletti (Research Scientist)
Clyde M. Wyman (Research Technologist)
H.M. Reynolds (Research Technologist)

Students:

B.T. Marshall, M.S. degree (December 1981)
Thesis title: Characterization and Regional Climatic Implications of Tropospheric Aerosols

B.B. Murphey, M.S. degree (in progress)
Tentative Thesis title: An Investigation on Methods of Determining the Optical Absorption Coefficient of Aerosols

PUBLICATIONS BASED ON WORK DIRECTLY SUPPORTED BY THIS GRANT

A. Coletti, Light scattering by non-spherical particles: a laboratory study. To be submitted to Aerosol Science and Technology (a copy is included as Appendix II)

PUBLICATIONS BASED ON WORK INDIRECTLY SUPPORTED BY THIS GRANT

G.W. Grams, 1980: In-situ light scattering techniques for determining aerosol size distributions and optical constants. In Light Scattering by Irregularly Shaped Particles (D.W. Schuerman, Ed.), Plenum Press, New York, pp.243-246.

G.W. Grams and A. Coletti, 1982: Analysis of polar nephelometer data obtained at the First International Workshop on Light Absorption by Aerosol Particles. In Light Absorption by Aerosol Particles (H.E. Gerber and E.E. Hindman, Eds.) Spectrum Press, Hampton, Virginia, pp.251-266.

E.M. Patterson, B.A. Bodhaine, A. Coletti, and G.W. Grams, 1982: Volume scattering ratios determined by the polar and the integrating nephelometer: a comparison. Appl. Opt., 21, 394-397.

E.M. Patterson and B.T. Marshall, 1981: Diffuse reflectance and diffuse transmission measurements of aerosol absorption at the First International Workshop on Light Absorption by Aerosol Particles. Appl. Opt., 21, 387-393.

BIBLIOGRAPHY

Baker, M.B. and A. Coletti, 1982: Uncertainties in the evaluation of shortwave radiative properties of an aerosol layer due to experimental and numerical errors. Appl. Optics, 21, 2244-2252.

Berglund, R.N. and B.Y.H. Liu, 1973: Generation of monodisperse aerosol standards. Environ. Sci. Technol., 7, 147-153.

Gerber, H.E. and E.E. Hindman (Eds.), 1982: Light Absorption by Aerosol Particles, Spectrum Press, Hampton, Virginia, 420pp.

Grams, G.W., A.J. Dascher, and C.M. Wyman, 1975: Laser polar nephelometer for airborne measurements of aerosol optical properties. Optical Engineering, 14, 85-90.

Liu, B.Y.H., 1975: Standardization and Calibration of Aerosol Instruments. In "Fine Particles - Aerosol Generation Measurements, Sampling and Anlysis", B.Y.H. Liu, Editor, Academic Press, pp. 39-53.

Pinnick, R., D.E. Carroll, and D.T. Hoffman, 1976: Polarized scattering from monodisperse randomly oriented non-spherical aerosol particles: measurements. Appl. Opt., 15, 384-393.

Pollack, J.B. and J.N. Cuzzi, 1980: Scattering by nonspherical particles of size comparable to a wavelength: a new semi-empirical theory and its application to tropospheric aerosols. J. Atmos. Sci., 37, 868-881.

Zerull, R.H., 1976: Scattering measurements of dielectric and absorbing nonspherical particles. Beitr. Phys. Atmosph., 49, 169-188.

APPENDIX I.

Non-Spherical Aerosol Particles Obtained With The Vibrating Orifice Generator

Sodium Chloride

Sodium chloride (complex refractive index = 1.54) crystallizes in spherical shells made of right parallelepipeds as shown in Figure 2a. At low values of concentration this quasi-regular structure seldom occurs and structures like those shown in Figure 2b (left) are more likely to occur.

Table I shows the numerical volumetric concentrations obtained in our laboratory, the actual minimum and maximum sizes determined by analyses of SEM photographs, and brief comments on the particle shape at each concentration.

Table I

Sodium Chloride

$m = 1.54 @ \lambda = .633\ \mu m$; $\rho = 2.165\ g\ cm^{-3}$

Concentration	Expected Equivalent Diameter (μm)	Observed Sizes (μm)	Comments
6.6×10^{-6}	0.78	1.3 - 1.5	Like in Fig. 1b
6.9×10^{-6}	0.8	1.0 - 2.1	Cubes
5.3×10^{-5}	1.6	1.6 - 2.3	Fig. 1b
8.3×10^{-5}	1.8	2.1 - 2.6	Like in Fig. 1a
4.2×10^{-4}	3.1	4.4 - 4.8	Like in Fig. 1a
6.7×10^{-4}	3.7	4.7 - 4.9	Fig. 1a
6.3×10^{-3}	7.7	5.2 - 5.9	Like in Fig. 1a

SODIUM CHLORIDE PARTICLES

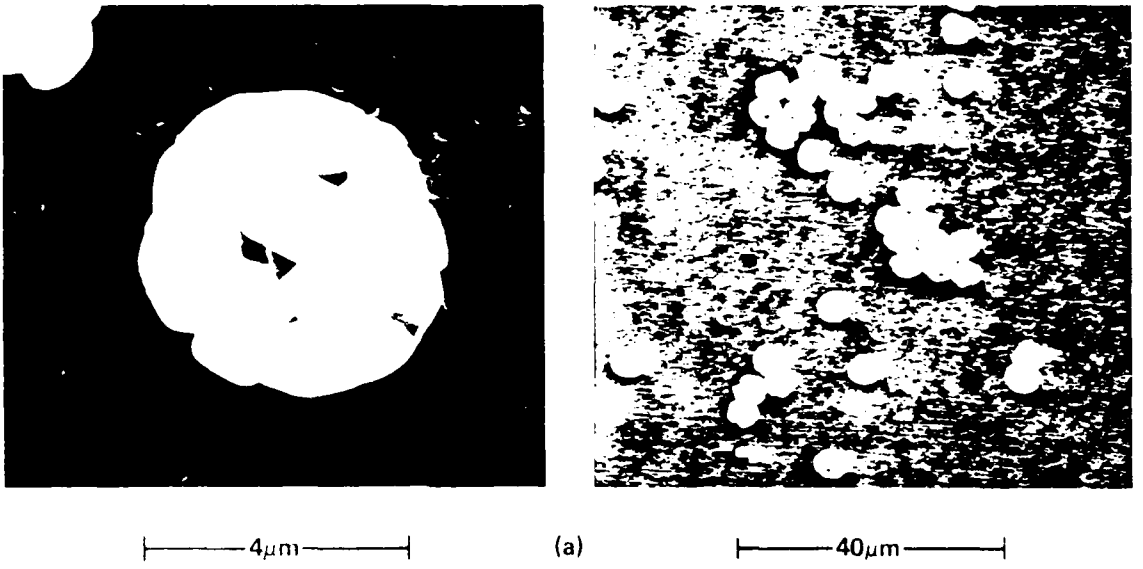

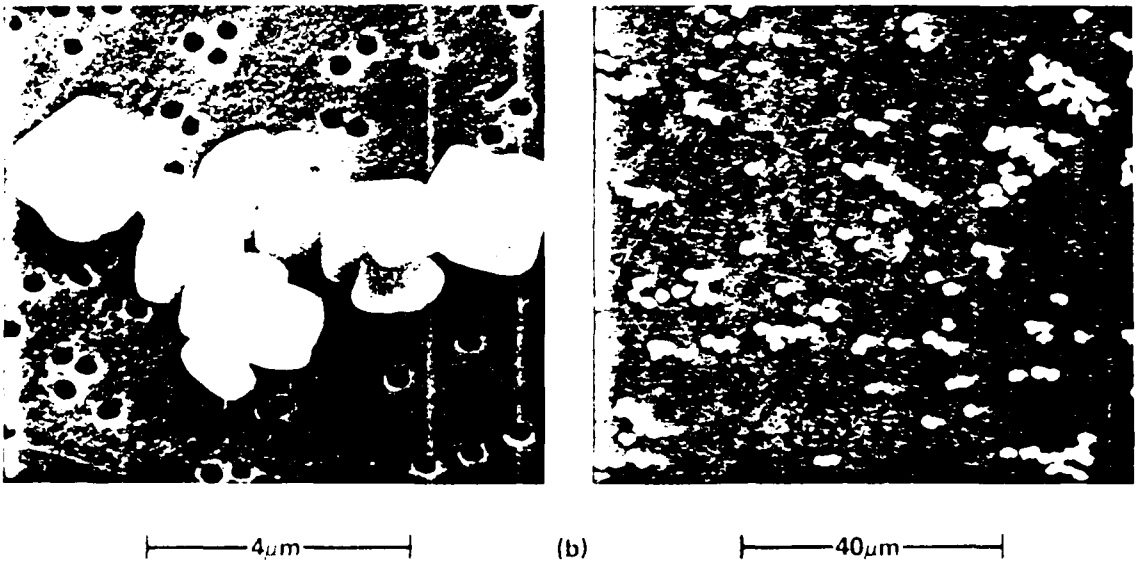

[illegible] Sodium chloride particles: (a) and (b). While the crystal [illegible] the crystal is similar to that shown in (a), [illegible] single cubes or several cubes together [illegible] the time as shown in (a).

Ammonium Sulfate

Ammonium sulfate (complex refractive index = 1.55) crystallizes in non-spherical particles formed by single or agglomerated round-edged crystals (Figure 3 and relative data in Table II). We have found indications from our optical measurements that this particle might be hollow. This fact has not been confirmed by other authors' observations.

Table II

Ammonium Sulfate

$m = 1.55$ @ $\lambda = .633$ μm; $\rho = 1.769$ g cm^{-3}

Concentration	Expected Equivalent Diameter (μm)	Observed Sizes (μm)	Comments
5.3×10^{-5}	1.6	1.9 - 2.3	Fig. 2a
8.3×10^{-5}	1.8	2.2 - 2.4	Like in Fig. 2a
4.2×10^{-4}	3.1	3.5 - 4.0	Fig. 2b
6.7×10^{-4}	3.7	3.2 - 4.0	Like in Fig. 2a

AMMONIUM SULFATE PARTICLES

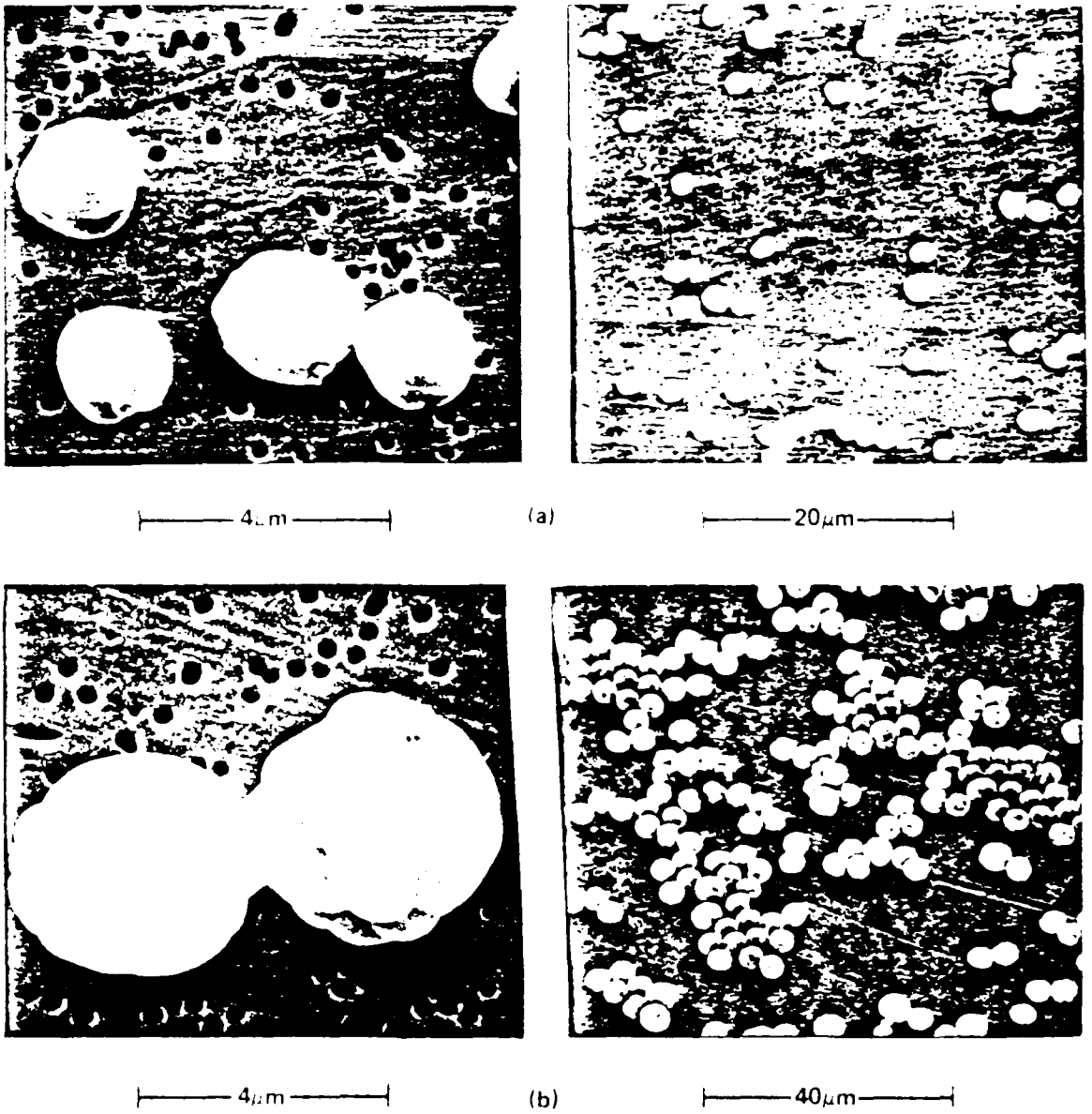

Potassium Chlorate

Potassium chlorate (complex refractive index = 1.48) crystallizes in spheres marked with wrinkles of variable shape and depth that give a characteristic aspect (Figure 4a). We have found some indications of the presence of internal marked dishomogeneities. This interpretation is supported by observations of the manner in which the fragile particles broke on impacting the filter (Figure 4b). Discussions by other authors also tend to confirm this interpretation.

Table III

Potassium Chlorate

$n = 1.682$ @ $\lambda = .633$ μm; $\rho = 2.32$ g cm^{-3}

Concentration	Expected Equivalent Diameter (μm)	Observed Sizes (μm)	Comments
6.66×10^{-6}	0.78	1.1 - 1.3	Like in Fig. 1e
5.3×10^{-5}	1.6	2.2 - 2.3	Fig. 3a
6.7×10^{-4}	3.7	4.2 - 4.5	Fig. 3b

POTASSIUM CHLORATE PARTICLES

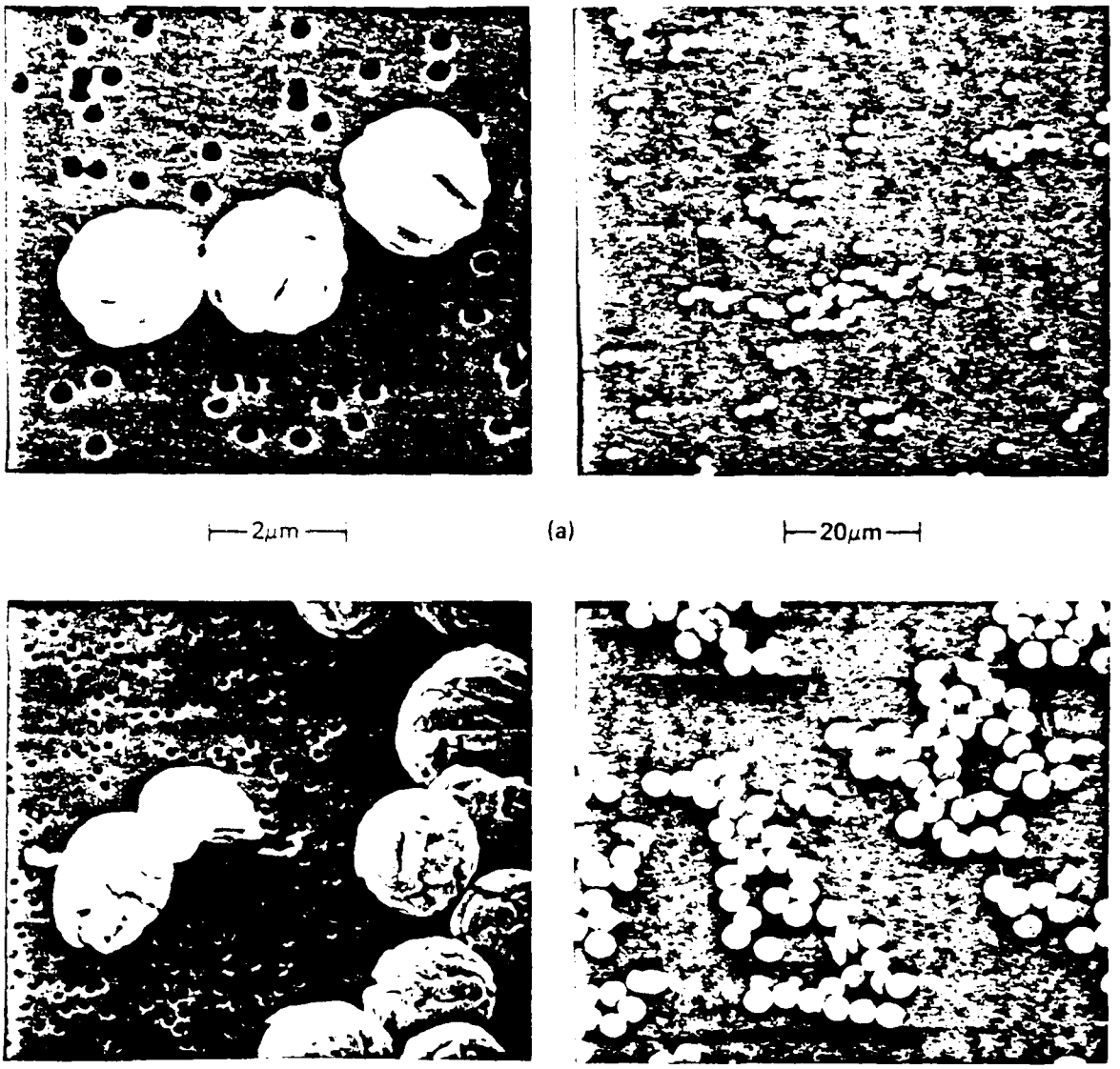

[illegible] droplets crystallize in quasi-spherical particles [illegible] perhaps they are agglomerates of [illegible] attained in a relatively irregular structure as [illegible] seem to indicate.

Methylene Blue

The complex refractive index of Methylene Blue is not well known. Patterson et al. (1981), recommended 1.67 - 0.2i on the basis of diffuse transmission measurements. For our data analysis, we used 1.67 - 0.6i on the basis of comparisons between the measured phase functions and those calculated from Mie theory for spherical particles.

With this compound, it often proved to be difficult to start the liquid jet of the aerosol generator. We associate this with an increased value of surface tension of the liquid that tends to markedly decrease the flow through the liquid filter of the syringe. The addition to the solution of a little more ethanol was usually enough to solve the problem. This procedure, however, caused some uncertainty in the recorded values of concentration and our expected equivalent particle sizes are less reliable for this compound as compared with our other experiment.

Table IV

Methylene Blue

$m = 1.67 - i\begin{matrix}0.6\\0.2\end{matrix}$ @ λ = .633 μm; ρ = 1.47 g cm^{-3}

Concentration	Expected Equivalent Diameter (μm)	Observed Sizes (μm)	Comments
1.04×10^{-5}	0.93	0.99 - 1.14	Like in Fig. 4a
5.3×10^{-5}	1.6	1.0 - 1.2	Like in Fig. 4a
8.3×10^{-5}	1.8	1.6 - 2.2	Fig. 4b
6.7×10^{-4}	3.7	3.0 - 3.6	Fig. 4a

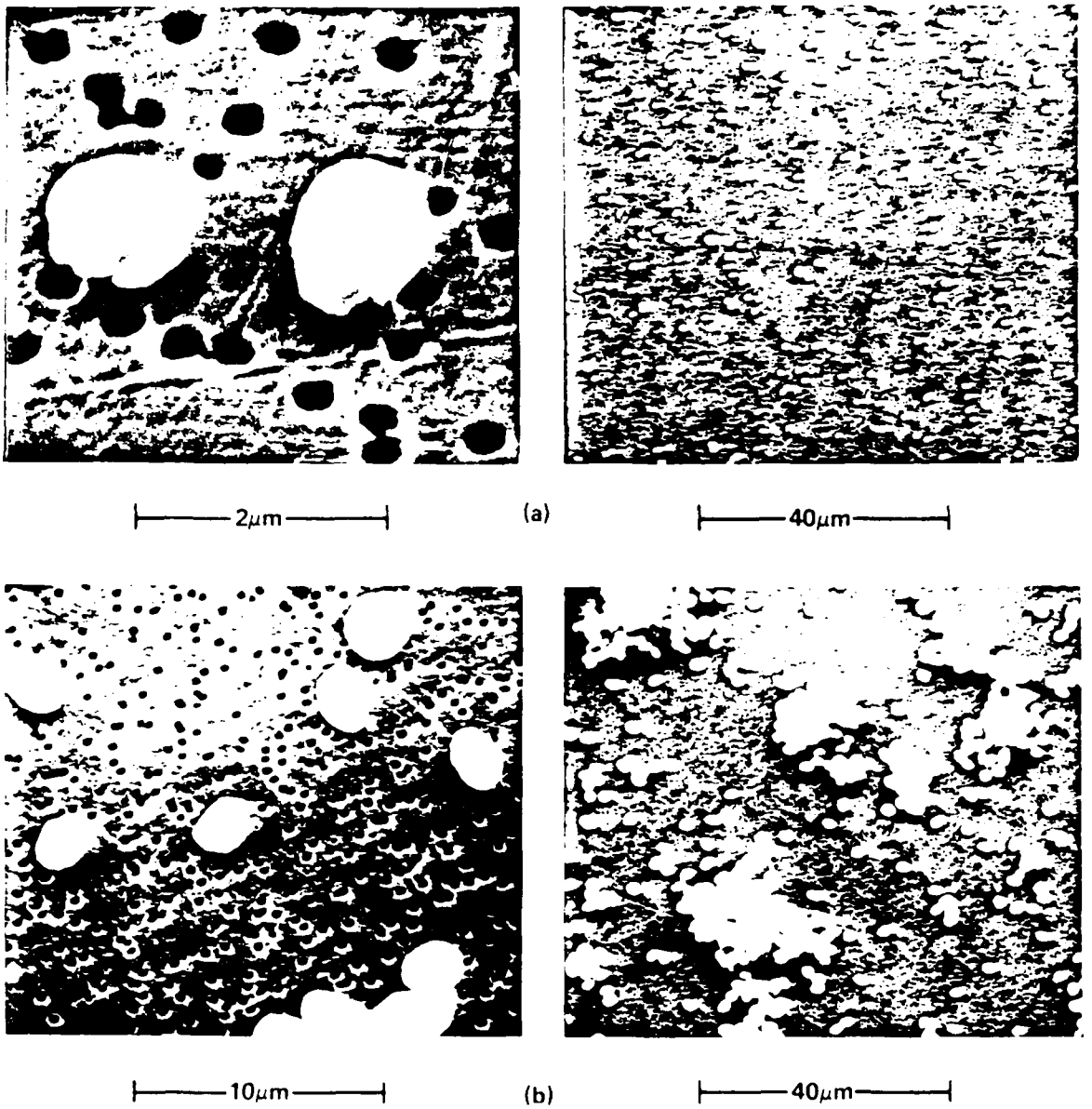

Figure 1. Methylene blue droplets dry out leaving irregular quasi-spherical shapes. At visible wavelengths their surfaces can hardly be approximated as smooth (a, b). The example on the right in (b) demonstrates that methylene blue particles have a tendency to agglomerate on the filter.

Nigrosine Dye

Nigrosine dye particles had characteristics very similar to those of Methylene Blue in the way they crystallize (Figure 6, left side). Pinnick has suggested a value of 1.67 - .026i (± 5%) on the basis of diffuse reflectance measurements. Our best-fit refractive index values, based on phase function comparisons with Mie theory were 1.67 - 0.6i.

As an operational procedure, it is recommended that the solutions be prefiltered before loading them in the aerosol generator. Some ethanol can be added either to replace the solvent that evaporated during the filtering process or if, as in the case of Methylene Blue, the surface tension of the solution does not allow sufficient flow through the system.

Before and after experiments with Nigrosine dye, we found it very helpful to wash the aerosol generator with methanol instead of isopropyl alcohol. Isopropyl alcohol, recommended in the manual of the generator as a general purpose solvent, is not a good solvent for Nigrosine dye. Therefore, either ethanol or methanol or water was found to be preferable.

Table V

Nigrosine Dye

$m = 1.62 - i\begin{{0.6}\\{0.26 \pm 5\%}}$; $\rho = 1.67$ g cm^{-3}

Concentration	Expected Equivalent Diameter (μm)	Observed Sizes (μm)	Comments
6.6×10^{-6}	0.78	1.0 - 1.2	Like Fig. 5a
1.04×10^{-5}	0.93	0.9 - 1.1	Like Fig. 5a
5.3×10^{-5}	1.6	1.8 - 2.4	Fig. 5a
8.3×10^{-5}	1.8	2.3	Like Fig. 5a
4.2×10^{-4}	3.1	2.7 - 4	Like Fig. 5b
6.7×10^{-4}	3.7	3.4 - 5	Fig. 5b

NIGROSINE DYE PARTICLES

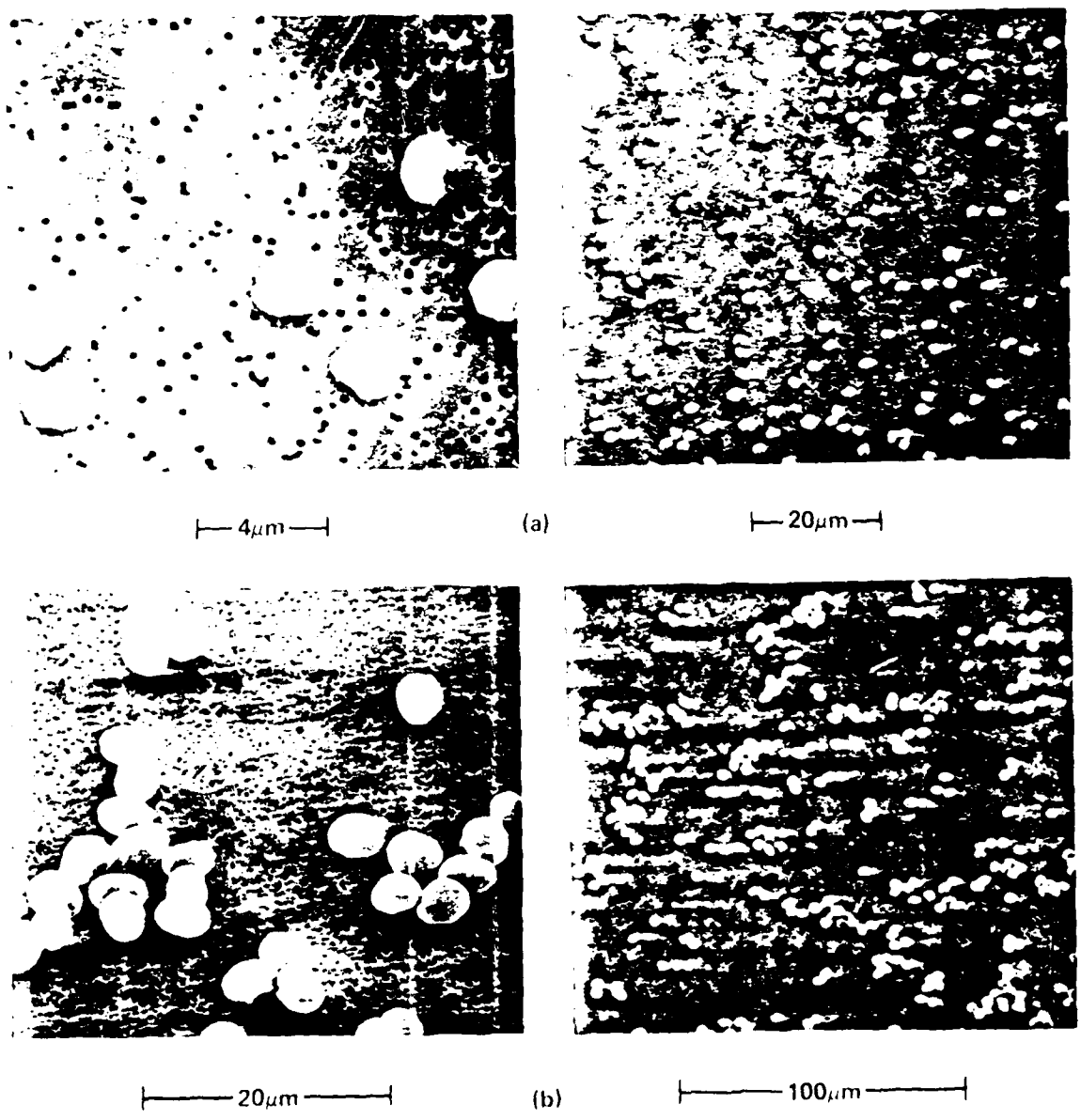

Figure 1. Nigrosine dye particles are usually near-spherical or ellipsoidal with irregular surface characteristics (a), but they may have a "grape"-like clump with crate on the filter is shown on the right in (b).

Mixed Solutions of Ammonium Sulfate and Nigrosine Dye

In terms of the generation of non-spherical crystals, mixed solutions of these two compounds can give very interesting results. Figure 7(a) shows the particles obtained for solutions with 75% ammonium sulfate and 25% nigrosine dye. Figure 7(b) shows the particles obtained for solutions with 25% ammonium sulfate and 75% nigrosine dye. Solutions made with equal parts of each salt had intermediate characteristics. We consider this shape of particle typical for the mixtures because they reproduce fairly well, as shown in Table VI. No information is available at present for representative effective values of refractive index for these solutions.

Table VI

Mixed Solutions of Ammonium Sulfate and Nigrosine Dye

Concentration	Expected Equivalent Diameter (μm)	Observed Sizes (μm)	Comments	
6.6×10^{-6}	0.78	1.0 - 3.0	Like Fig. 6a	75% Ammonium Sulfate and 25% Nigrosine dye
5.3×10^{-5}	1.6	1.0 - 2.7	Like Fig. 6a	
6.2×10^{-4}	3.1	2.7 - 4.0	Like Fig. 6a	
6.6×10^{-6}	0.78	0.8 - 1.1	Irreg. Like Fig 6b	50% Ammonium Sulfate and 50% Nigrosine dye
5.3×10^{-5}	1.6	1.5 - 2.5	Like Fig. 6b	
6.2×10^{-4}	3.1	4.0 - 6.3	Dried Fruits Fig. 6b	
6.6×10^{-6}	0.78	1.0 - 1.4	Figure 6b	25 Ammonium Sulfate and 75 Nigrosine dye
5.3×10^{-5}	1.6	1.0 - 2.9	Figure 6b	
6.2×10^{-4}	3.1	4.5 - 5.6	Figure 6b	

AMMONIUM SULFATE AND NIGROSINE DYE MIXTURES

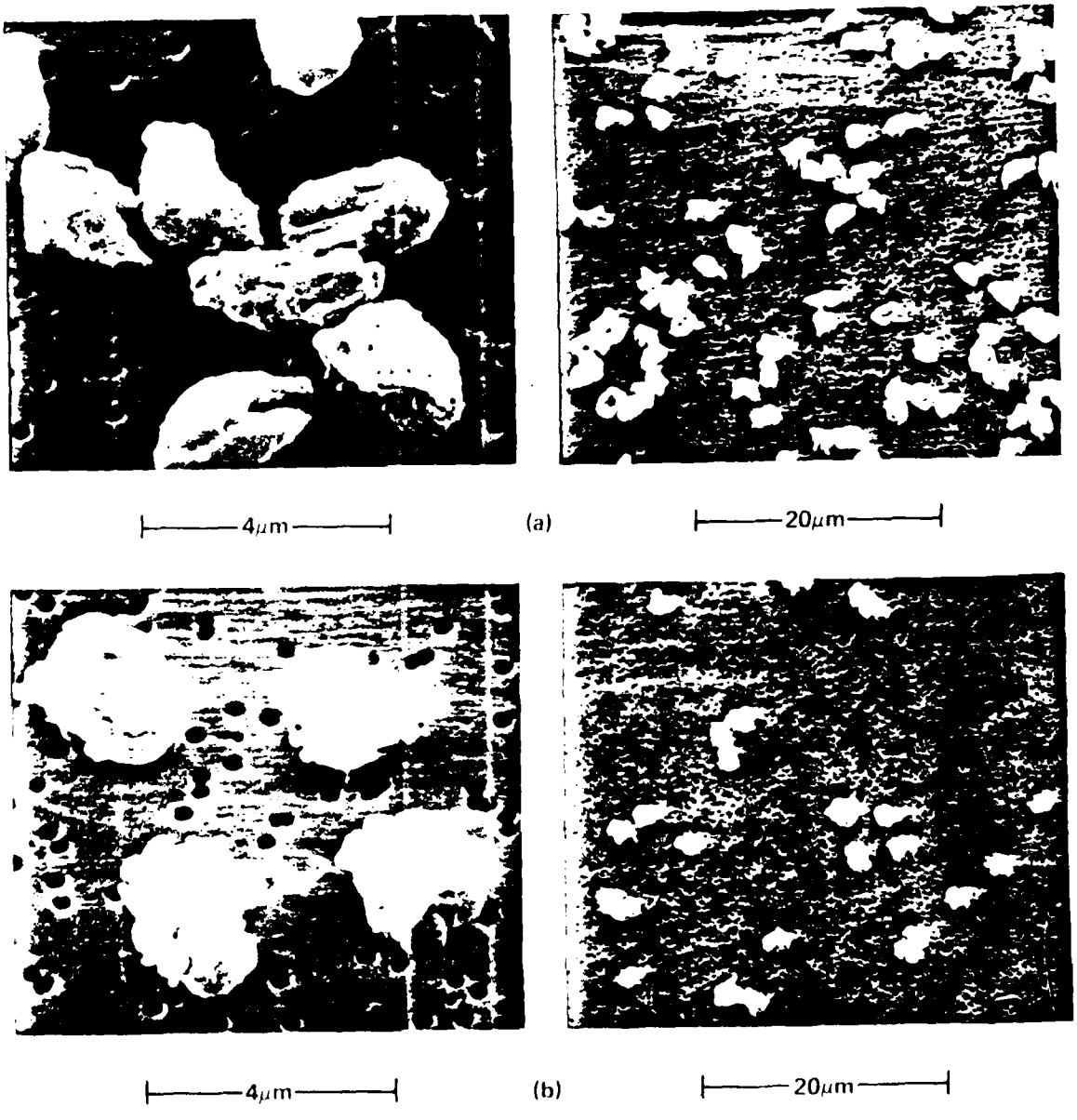

Figure 1: Mixtures of ammonium sulfate and nigrosine dye assume irregular shapes resembling dried fruits with characteristics varying almost [illegible] between the two compounds. The example shown in (a) is typical for solutions of 75 ammonium sulfate and 25 nigrosine dye while the example in (b) is for solutions of 25 ammonium sulfate and 75 nigrosine dye.

APPENDIX II

Light Scattering by Non-Spherical Particles: A Laboratory Study

A. COLETTI

Georgia Institute of Technology - School of Geophysical Sciences
Atlanta, Georgia 30332

To be submitted to

Aerosol Science and Technology

Light Scattering by Non-Spherical Particles: A Laboratory Study

A. Coletti

Georgia Institute of Technology - School of Geophysical Sciences
Atlanta, Georgia 30332

ABSTRACT

The concept of dividing the light scattering by non-spherical particles into three components - diffracted, refracted and reflected - is discussed here in the case of monodisperse aerosol particles using a set of measured phase functions. A logical scheme is developed that allows a simple representation of the light scattering properties of classes of non-spherical particles in a region where geometric optics is not expected to be valid. In the limits of this analysis, it appears that the equations developed can be applied to larger varieties of problems where there is a need to infer the optical properties of non-spherical particles.

1. INTRODUCTION

The properties of light scattered by suspended dust particles is of interest in different fields. In some cases, light sources of known characteristics are used to obtain information on the physical and chemical nature of aerosols; in others, suspended dust masks the properties of partially known light sources. For example, various models of dust particles are hypothesized in infrared astronomy in order to explain the high emissivity of certain Nebulae

(e.g., Rowan-Robinson[1]) and interplanetary dust grains have been studied through observations of zodiacal light. In the atmosphere, where non-spherical dust particles are commonly present, studies of the dependence of radiative transfer models on the asymmetry factor and single scattering albedo (the average cosine of the scattering angle and the ratio of scattering to extinction) have shown that, under certain circumstances, these two parameters need to be evaluated with a precision of few percent (see, e.g., Baker and Coletti[2]).

Light scattering processes are controlled by the ratio between the size of the particles and the wavelength of the light source, by the complex refractive index, and by the morphology of the particles. The large varieties of shapes and chemical compositions of particles in nature and the formal and numerical complexities of rigorous solutions of the Maxwell equations, make exact calculations impossible in many cases.

Precise and systematic experimental studies of electromagnetic scattering have been made by Zerull[3] and by Schuermann et al.[4] using microwave techniques and suspended objects of various shapes and chemical compositions. Visible light and laboratory-generated aerosols have been used by different authors (Powell et al.[5]; Holland and Gagne[6]; Napper and Ottewill[7]; Cross and Latimer[8]; and Pinnick et al.[9]) to study different shapes of particles in the size range where the Mie theory for spherical particles is no longer a reasonable approximation. These experiments showed basic differences between the light scattering properties of non-spherical particles and analogous Mie spheres for sizes of the order of two or three times the wavelength. Basically the light intensity, as a function of the scattering angle, does not vary as much as in the spherical case, and it is less sensitive to the light polarization.

Subsequent to these observations, Pollack and Cuzzi[10] formulated a semi-empirical theory to describe the light scattering by polydisperse size distributions of particles of arbitrary shapes. They assumed a linear combination of Mie spheres and of particles that are diffracting, reflecting, and transmitting light, obeying the laws of classical optics. In attempting to provide a fitting procedure, Pollack and Cuzzi observed that, in the analyzed cases, the two parameters, asymmetry factor and single scattering albedo, were significantly affected by the morphological properties of the particles. Indirectly, the same observation was made by Pinnick et al.[4], who compared the light scattering of partially empty crystals with that of spherical shells.

In the first part of this article, the experimental set-up used by Coletti and Evans[11] to study light scattering by non-spherical particles of known chemical composition is briefly described. The second part discusses the method used for the data analysis in order to obtain proper normalization of the data and to estimate the asymmetry factor parameters. In the third part, examples of experimental data are reported, along with a discussion of a best-fitting procedure that, analogous to Pollack and Cuzzi, uses the diffraction and reflection equations to describe portions of the measured phase functions. The purpose of this section will be essentially to show the basic processes active in light scattering by non-spherical, absorbing and non-absorbing particles, in order to justify the assumptions made in the following section. In the fourth part, the physical observations are organized into a simple scheme which, even though extremely simplified, predicts the optical properties of particles of certain shape categories.

2. EXPERIMENTAL SET-UP

Since the objective of our set of measurements was to study the light scattering properties of particles of definite shape and chemical composition, we used laboratory-generated monodisperse aerosol particles. As shown by Pinnick et al.[7] and Liu[12], a vibrating orifice aerosol generator produces basically monodisperse aerosol particles. A solution of known concentration of a salt is forced through a small orifice driven by a piezo-ceramic that vibrates at a specified frequency. The resulting jet breaks up into droplets of uniform size under the combined effects of surface tension and mechanical perturbation. A relatively strong stream of dry, filtered air evaporates the solvents and dilutes the aerosol in order to minimize coalescence and coagulation of the particles. These two combined effects are such that the resulting size distribution, as observed with a scanning electron microscope (SEM), has about 10 % of particles with volume double those in the main population. Because the scattering process is basically proportional to the cross section of the particles, the droplets will increase the light scattering of the sample by 15 or 20 %.

Once generated, the aerosol passes through the laser polar nephelometer described by Grams[13,14] which measures the light scattered by aerosol particles in two orthogonal planes of polarization at scattering angles between 10 and 170° in steps of 5°. The laser source is polarized either in the horizontal or perpendicular plane of reference of the laboratory and operates at a wavelength of .633 μm. During each experiment, between 10 and 40 angular scans were taken so that the experimental points in the figures of phase functions

presented, represent the average over the total number of measurements; the error bars denote the variance.

The experimentation included light scattering measurements on particles generated from three non-absorbing salts (sodium chloride, ammonium sulfate, and potassium chlorate) and two high absorbing compounds, methylene blue (MB) and nigrosine dye (ND).

3. DATA ANALYSIS PROCEDURE

The polar nephelometer measures the light diffused by the aerosol particles at each angle θ for two orthogonal planes of polarization of the light. Designating the polarization planes by the index i (= 1,2), the signal $s_i(\theta)$ detected by the instrument (corrected by the $\sin\theta$ effect of the field of view) is proportional to the number N of particles crossing the illuminated volume, their area A, scattering efficiency Q_{sca} and normalized phase function $P_i(\theta)$. That is:

$$s_i(\theta) = D\, N A\, Q_{sca}\, P_i(\theta) \quad , \tag{1}$$

where D is the sensitivity of the instruments.

The quantities A, Q_{sca} and $P_i(\theta)$ depend on the size and shape of the particles (which are asumed randomly oriented). Q_{sca} and $P_i(\theta)$ depend also on the complex refractive index $m = (n - 2k)$ which, in turn, is related to the chemical composition of the particles.

While the quantity D is obtained from our instrumental calibration procedure, the measurement of the total number of particles N is troublesome.

Therefore, only the product N A Q_{sca} is obtainable with an appropriate choice of the normalization factor for $P_i(\theta)$ defined such that:

$$\frac{1}{2} \int_0^{\pi} (P_1(\theta) + P_2(\theta)) \sin\theta d\theta = 2. \qquad (2)$$

In our measurements (taken every 5° between 10 and 170°), we chose to compute the normalization factor η using the formula:

$$P_i(\theta) = \frac{2 s_i}{\eta} . \qquad (3)$$

That is:

$$\eta = \frac{1}{2} \cdot \left(\sum_{i}^{n} \frac{\Delta\theta}{3} w_i s_i (\theta_i) \sin\theta_i + \varepsilon_f + \varepsilon_b \right) \qquad (4)$$

w_i are the weights of the Simpson summation rule, and ε_f and ε_b are the contribution to the normalization constant arising from the two regions 0-10° and 170-180°, where measurements are not available.

It has been shown that a similar problem arises computing the value of the asymmetry factor G from the measurements. The asymmetry factor is a parameter often used in radiative transfer models[4,5], and is defined as average value of the cosine of scattering:

$$G = \frac{1}{2} \int_0^{\pi} \frac{(P_1(\theta) + P_2(\theta))}{2} \sin\theta\cos\theta d\theta. \qquad (5)$$

In analogy to Eq. (3), we can carry out a numerical summation of the experimental data to obtain an estimate of G from an equation of the form

$$G = \frac{\sum_{i=1}^{n} \sum_{j=1}^{m} w_i s_1(\theta_j) \sin\theta_j \cos\theta_j \Delta\theta_i \Delta\theta_j}{2\sigma} \qquad (6)$$

where ε_a and ε_b are again the contributions arising from the regions not covered by the angular scans.

In the case of spherical particles, calculations made using the Mie theory show that for a reasonable range of refractive indices, the error due to the angular truncation is greater than the expected experimental error for values of the size parameter x (the ratio $x = 2\pi r/\lambda$ between 2 times the radius of the particle and the wavelength) greater than 5. For a size parameter equal to 20, the contribution of the scattering between 10 and 170° is of the order of 0.5 %. So an accurate accounting for scattering between 0 and 10° is needed.

The forward scattering peaks of highly absorbing particles of general shape are rigorously described by the diffraction law (see e.g., Born and Wolf[9], p.539). In the case of refracting spheres, the peaks are the result of interference between diffraction and refraction, as noted, for example, by Hansen and Travis[7]. The diffraction formula can still be considered a good approximation (Hotkinson and Greensleaves[10], Kerker[2], Pollack and Cuzzi[10]) but the best fitting size parameter x_d will be slightly different from the true Mie size parameter x_{Mie}. In fact, the first minimum in the diffraction formula coincides with the first zero of the Bessel function of the first kind, given by:

$$x_d \sin\theta = 2x_d \sin(\theta/2)\cos(\theta/2) = 3.83 \qquad (7)$$

and, in first approximation, the first minimum of the Mie theory (for real refractive index $n = 1.3$) is given by[11]:

$$x_{Mie} \sin(\theta/2) = 3.566/\qquad (8)$$

Consequently, we have:

$$x_{Mie} = 0.92\, x_d \cos(\theta/2) \quad . \tag{9}$$

For highly non-spherical randomly oriented particles, the diffraction is not related any longer to a single value of size, but to all the possible cross sections obtainable from different orientations of the particles. In the figures presented in this article, this effect has been disregarded because we consider only particles that, in the measured forward portion of the phase function, give rise to well-defined diffraction peaks.

We computed the quantities θ_f and θ_f with the following numerical procedures:

1. Determination from the measurements of the angle interval where the first minimum in the diffraction peak occurs.
2. Definition of the range of possible size parameters x_d from the position of this minimum and the information on the size of the particles as obtained from the SEM picture.
3. Comparison with the Fraunhofer diffraction formula[10]:

$$i_d(\theta, x_d) = c_d \left[\frac{2 J_1(x_d \sin\theta)}{x_d \sin\theta} \right]^2 (1 + \cos^2\theta) \tag{10}$$

   of the best-fitting values of x_d and of the normalization factor c_d. In this equation, $J_1(x_d \sin\theta)$ represents the Bessel function of the first kind.

4. Evaluation of the two integrals:

$$\chi_f = \int_{\theta_0}^{\pi} f_d(\theta, x_d) \sin\theta\cos\theta\, d\theta \qquad (11)$$

$$\chi_f = \int_{\theta_0}^{\pi} f_d(\theta, x_d) \sin\theta\, d\theta \,. \qquad (12)$$

and $\theta_0 = 170/180$.

In the backward direction, the contributions of χ_b and γ_b are much less critical and the phase functions of non-spherical particles always present a smoothed and regular slope. Therefore, a simple linear interpolation formula for the integrand in (11) and (12) in the region 170-180° appeared to be the best way to evaluate χ_b and γ_b.

Figure 1 shows the comparison between the results of the Mie theory for particles of nigrosine dye of size parameter 9.4 (complex refractive index $m = 1.67 - i\,0.6$) and the experimental values of the measurements, normalized in the way just described. The shape of the particles generated is shown in the insert of the figure. Their minimum and maximum size parameters are 9.2 and 11.0. The extrapolated value of the asymmetry factor in this case is $g = 0.864$ while the Mie theory gives $g_{Mie} = 0.875$. Without the correcting terms χ_f, γ_b, and χ_f and γ_b, we would obtain an approximate value of 0.815. Because of the high light absorption of the nigrosine dye (estimated imaginary part of the complex refractive index $\nu = 0.6$) the value of the Mie size parameter and of the diffraction size parameter are practically the same.

4. DISCUSSION OF SOME TYPICAL PHASE FUNCTIONS

Typical examples of experimental results obtained for light absorbing and for light absorbing aerosols, are shown in Fig. 2 and Fig. 3; Figure 2

represents the measured phase function for non-absorbing particles of NaCl of minimum and maximum dimensions, estimated from the SEM picture, equal to 2.7 - 3.0 μm. Figure 3 is the phase function for absorbing particles of methylene blue of minimum and maximum axis 1.6 - 2.2 μm. Comparing these two figures, we notice how, in the forward portion of scattering, both kinds of particles present peaks that could be described as due, basically, to diffraction (represented by the dotted line in the figures), while in the other directions, they follow different patterns. For non-absorbing materials, the fraction of light reflected by a surface is at the most of the order of 10% of the refracted fraction; the refracted light, crossing absorbing materials, decays proportionally to exp (-2x) so that it is practically completely absorbed at optical thickness two or three, as for particles of Fig. 3. While the particles of MB appear to be slightly rough, amorphous crystals, the particles of sodium chloride are a shell-like combination of crystals so that diffuse reflection can occur on their surface.

Figure 4a shows the angular dependence of the Fresnel fraction of reflected energy for spheres with refractive index of sodium chloride (m = 1.54 - 0 i) and Fig. 4b for spheres with refractive index m = 1.55 - 0.5i. These fractions depend on the complex refractive index and on the shape of the particles; they do not depend on the size, but are influenced by the roughness of the surface (compared with the wavelength). The fraction of reflected light with transverse electric vector has a minimum (at the Brewster angle of the material) while that with perpendicular electric vector increases for decreasing angles of scattering.

The similarity between the reflectivity curve in Fig. 4b and the phase function of the particles of MB confirms the idea that the reflected component

predominates at large scattering angles while it is weak in the case of sodium chloride crystals. It is also interesting to note that the refracted unpolarized light of sodium chloride has an angular dependence similar to the perpendicular reflected component, so that reflection and refraction are practically indistinguishable if the light is unpolarized as in the case discussed by Pollack and Cuzzi[1].

The light refracted by a randomly oriented non-spherical particle cannot be described by an exact formula, therefore, we arbitrarily chose to fit this component with an Henyey-Greenstein phase function[10]:

$$f_{HG}(\Theta,g) = (1 - g^2)/(1 + g^2 - 2g\cos\Theta)^{3/2} \qquad (13)$$

where g is a parameter that controls the slope and is also the asymmetry factor of the function. This choice has the advantage that it has historically proven helpful in describing different kinds of scattering processes[11].

The Henyey-Greenstein phase function can fit the refracted light as computed from ray optics for spheres, but is unpolarized, so it is appropriate for the process of multiple internal reflections from randomly oriented surfaces. In addition, this phase function with suitable choice of g, can also resemble the unpolarized Fresnel reflection formula, as it is required by the observation made on the refracted and reflected light in the case of sodium chloride.

Fig. 5 and 6 show the results of a best-fitting routine, where we combined Mie scattering, diffraction, polarized reflection and an Henyey-Greenstein phase function to represent the experimental cases shown in Figs. 3 and 4. It has to be pointed out that this fitting procedure is not linear because the fraction of polarized light represented by the diffraction formula has been subtracted from the refracted components for the reasons already mentioned. In Fig. 5, that is a particle of NaCl, the diffracted component, C_d, contributes 28% of the total light scattering. The coefficient of the

Henyey-Greenstein phase function c_t is 54% and it is related to refraction and diffuse reflection (but not refraction interfering with diffraction) while the reflection coefficient c_r, accounting for reflection by smooth surfaces, is only 1% .

The disagreement in Fig. 5 between the measured backscattering and that computed for the best-fitting curve, indicates that some other process is active in this region of scattering. In the case of the spheres, the high backscattering is basically due to combinations of external and multiple internal reflections. In the case of non-spherical particles, this process could probably be treated with models of light reflected by rough surfaces, as proposed by Mukai and Mukai[7].

In Fig. 6, that is for methylene blue, the major contributions are from pure diffraction ($c_d \cong 75\%$) and polarized reflection ($c_r \cong 25\%$).

Table I lists the coefficients obtained fitting the set of measured phase functions for aerosols of sodium chloride of different sizes. Presented for each particle size is the size observed by SEM, the best-fitting Mie theory size parameter (if such determination was possible), the size parameter obtained from the best-fitting curve, and the values of the asymmetry factors: that for the Henyey-Greenstein phase function g; that computed from the experimental data in the interval 10-170°, $\bar{g}$; and that obtained with the extrapolation, C. A few comments on this table are necessary:

a) the observed size of the particles x_{SEM}, actually defines an interval because in the pictures the particles appear irregular;

b) the measured peaks of the phase functions determined the size of the particles more precisely than the pictures, but still not enough to allow us to resolve the mentioned systematic differences between x_{Mie} and x_d, without careful numerical evaluation;

c) the value of a turned out not to be critical for the best-fit and always ranged around the value of 0.4. The same is true in the case of the other non-light absorbing salts, though for slightly different mean values of q.

Comparing the values of the coefficients c_d, c_t and c_r in Table 1, it can be observed that the reflected component, c_r, contributes less than the others to the measured phase functions. Therefore, in order to obtain information in the first approximation, on the relative variations of diffracted and transmitted components as function of size, we can keep this coefficient constant and equal to zero so that:

$$c_d = 1 - c_t \qquad (3.1)$$

Fig. 7a shows the best fitting values assumed under this condition by the coefficients c_d (ordinate axis on left) and c_t (ordinate axis on right).

In the case of spherical non light absorbing particles, the major oscillations in the curve of the extinction coefficient, as a function of the size parameter, can be explained as due to constructive and destructive interference of diffracted and transmitted light[16]. The same effects explain also the main oscillations present in the curve of the asymmetry factor[17]. Figure 7b shows the experimental values of the asymmetry factor G, as function of the size parameter x_d, along with the curve of the asymmetry factor, computed with the Mie theory for spherical particles of same size (assuming $x_{Mie} = x_d$) and complex refractive index m = 1.54. Comparing Fig. 7a and Fig. 7b, it can be seen that correlation exists between the values of G and those of the coefficients of

diffracted light e_d. Moreover, the values of G follow basically the same law of the Mie scattering asymmetry factor besides a constant shift on the x axis.

The pictures taken at the SEM of the particles of sodium chloride (see insert Fig. 2) show that this salt crystallized in quasi-spherical structures internally empty. For spherical particles, the maxima and the minima in asymmetry factor curves are always in the same position for different materials if plotted versus the parameter $x(m - 1)$. In fact this parameter, called phase shift, takes into account the real optical path of the refracted rays inside the particles. Moreover, different authors, discussing optical properties of non-spherical particles, have demonstrated that the size of irregular particles can be conveniently expressed by the radius of the sphere of equal volume (see, e.g., references 10, 23, 24, 25). Therefore, it is justified to shift the experimental values of the asymmetry factor along the x axis (dotted line in Fig. 7) in order to take into account the real average amount of bulk material transversed by the light rays.

To obtain the best estimate for this shift we computed the root mean square values of the distances between the set of experimental values of e_d and the theoretical curve q_{Mie}:

$$\text{r.m.s.} = \left\{ \frac{1}{q} \sum_{j}^{q} \frac{(G_j - q_{jMie})^2}{q_{jMie}^2} \right\}^{1/2} \tag{15}$$

where q is the total number of independent determinations of G. These r.m.s deviations are plotted in Fig. 8a for sodium chloride particles as functions of multiplying factor λ:

$$x_d = \lambda x_{Mie} \tag{16}$$

In the calculations the Mie theory asymmetry factors have been obtained as averages on a narrow size distribution of particles (a log-normal with relative variance of 5%), in order to avoid oscillations of the r.m.s. deviations with the "ripple" of the Mie theory. The figure shows that good agreement between theory and experimental values is found shifting the Mie curve by the factor 1.6.

Analogous considerations can be made on the set of experimental data obtained for ammonium sulfate and potassium chlorate aerosols. Fig. 8b shows the plot of the r.m.s. deviations between the asymmetry factors for particles of ammonium sulfate (complex refractive index 1.53; q = 9) and Fig. 8c for particles of potassium chlorate (complex refractive index 1.492; q = 3). Both Figs. 8b and 8c show a clear minimum for values of the multiplying factor ε about 1.5, but the pictures at the SEM of these aerosol particles (see typical examples in the inserts in Figs. 8b and 8c) did not show any visible indications of internal holes. If we think in terms of interferences between diffracted and transmitted light, we can consider Fig. 8b and Fig. 8c as evidence that internal empty spaces actually existed even though not externally visible.

Fig. 9a shows the comparison between the experimental values of the asymmetry factor in the case of rhodosine dye and the Mie theory curve for complex refractive index m = 1.67 - i0.6 (q = 6). This value of the complex refractive index has been chosen as the one that was providing the best approximation with the Mie theory for the set of measured phase functions. The asymmetry factor curve turns out to have no oscillations because of the strong light absorption occurring inside the particles. Consequently, in this case of rhodosine dye, the r.m.s. deviations between the asymmetry factors depends weakly on the multiplying factor, ε, as shown in Fig. 9b.

The experimental results obtained on aerosols of methylene blue (complex refractive index m = 1.55 - i0.6 and q = 8) had properties completely analogous to those discussed in the case of nigrosine dye.

5. A PHYSICAL APPROXIMATION

Our experimental results have demonstrated that the laws of geometric optics can be used to fit phase functions of non spherical particles but that the Mie theory is needed to compute the asymmetry factors or scattering coefficients. That is, in our size particle range, interferences occuring between the different components of the light, diffracted, refracted and reflected, do not support the assumption of non-coherency between the three components. We observed also that the principal interferences occuring in the experiments is that between diffracted and transmitted light in the forward direction.

If we express the intensity of light at a given point P illuminated by two coherent monochromatic waves as:

$$I(P) = I' + I'' + 2\cos(\varphi)\sqrt{I'I''} \qquad (17)$$

where I' and I'' are the intensities and φ the difference between the phases of the two waves, we have that, at a given angle θ, the scattered intensity is proportional to:

$$I_i(\theta) = I_{oi} NAQ_{sca} \{ f_d(\theta,x_d) + (1-\gamma)[t\, f_{HG}(\theta,q) + r_i(\theta,m)] + 2\cos(\delta(\theta)) \sqrt{\gamma(1-\gamma)} \sqrt{t\, f_{HG}(\theta,q)\, f_d(\theta,x)} \}, \quad i = 1,2 \tag{18}$$

where γ expresses the ratio between the light diffracted and that transmitted or reflected, and t is the fraction of light transmitted through the particle. Here, $\delta(\theta)$ is the angular difference between the phase of the diffracted and the refracted light; in general, δ is a function of the scattering angle θ and of the optical path traveled by the rays inside the particle. We assume here that the diffracted and the reflected light, indicated with $r_i(\theta,m)$ are incoherent.

In the previous section, it has been shown that the phase between the diffracted and refracted light in the main forward peak can be approximated by the phase of the axial ray through an equivalent volume sphere, so that at zero scattering angle we have:

$$\delta(\theta = 0) = \delta_0 + 2x_d(n_r - 1), \quad \delta = \delta \tag{19}$$

where n_r is the real part of the complex refractive index, δ is the value of the phase shift for which the extinction efficiency of the equivalent volume size sphere has the first maximum and γ is the multiplying factor as defined in the previous paragraph.

In the other directions, in analogy with the spherical case, the phase should increase quite rapidly with scattering angle. Empirically, this can be obtained by multiplying $\cos\delta_0$ with a Gaussian function, decreasing at the same rate as the diffraction formula. Therefore:

$$\cos \psi = e^{-(\psi/\psi_0)^2} \cos \psi_0 \qquad (20)$$

With the approximation on the first zero of the Bessel equation of the first kind mentioned in Eq (17):

$$\psi_0 = \arcsin (x_d/3.85) \qquad (21)$$

We also approximate t as equal to:

$$t = (1-r) \exp (-2 x_d n_i/\xi) \qquad (22)$$
$$r = (r_1 + r_2)/2$$

where r is the total reflectivity of a spherical particle and the exponential takes into account the internal absorption.

The asymmetry factor g of the $f_{HG}(\theta,g)$ is determined experimentally with the procedure of the previous section and is a quantity characteristic of the particle shape. Now we can define the following quantities (omitting the arguments of the functions):

$$q_d = \int_0^{\pi} f_d \sin\theta\cos\theta d\theta / \sigma_d$$

$$q_{t,r} = \int_0^{\pi} \frac{(t\, f_{HG} + r_1) + (t\, f_{HG} + r_2)}{2} \sin\theta\cos\theta d\theta$$

$$q_{d,t} = \int_0^{\pi} (t\, f_{HG})^{1/2} \sin\theta\cos\theta d\theta$$

$$\sigma_d = \int_0^{\pi} f_d \sin\theta\, d\theta = \text{constant}$$

$$
\begin{aligned}
{}^{\prime}t,r &= \int_{i_2}^{i} \left(t_{HG} + \frac{r_i + r_r}{2}\right)\sin\theta\, d\theta = \text{constant} \\
{}^{\prime}d,t &= \int_{i_2}^{i} \left(t_d\, t_{HG}\right)^{\frac{1}{2}} \sin\theta\, d\theta
\end{aligned}
\tag{23}
$$

so that the asymmetry factor, G, of our artificial phase function, measured or determined by the Mie theory, will be:

$$
G = \frac{r_d\, r_d + (1-r_d)\, r_{t,r} + 2\cos\left(\quad\right)\sqrt{r_d(1-r_d)}\; r_{d,t}}{r_d\, r_d + (1-r_d)\, r_{t,r} + 2\cos\left(\quad\right)\sqrt{r_d(1-r_d)}\; r_{d,t}}
\tag{24}
$$

That is, θ is uniquely determined as the solution of a rational equation of the kind:

$$
a\cos\theta + b\sqrt{(1-\cos^2\theta)} + c \tag{25}
$$

where a, b and c are:

$$
\begin{aligned}
a &= r_d\, r_d - r_{t,r} + 2(r_d + r_{t,r} - 1) \\
b &= 2\cos\left(\quad\right)\left(r_{d,t} - 1\right) r_{d,t} \\
c &= r_{t,r} - 2(r_d + r_{t,r})
\end{aligned}
\tag{26}
$$

In summary, if all the approximations made are reasonable, and this has still to be proven, we have constructed a phase function that is able to simulate the measured phase function for a convenient choice of the free parameter γ, and for given values of the size parameter x_{ij}, the multiplying factors r_{ij} and the complex refractive index m. In addition, it is possible to predict phase functions of particles with similar shape (same value of r_d) for all the other

$$\cos \psi = e^{-(\quad)^2} \cos \psi_o \tag{20}$$

With the approximation on the first zero of the Bessel equation of the first kind mentioned in Eq (17):

$$= \arcsin (x_d/3.85) \tag{21}$$

We also approximate t as equal to:

$$t = (1-r) \exp (-2 x_d n_i/\quad) \tag{22}$$
$$r = (r_1 + r_2)/2$$

where r is the total reflectivity of a spherical particle and the exponential takes into account the internal absorption.

The asymmetry factor g of the f_{HG} (,g) is determined experimentally with the procedure of the previous section and is a quantity characteristic of the particle shape. Now we can define the following quantities (omitting the arguments of the functions):

$$q_d = \int f_d \sin\cos d\theta / \quad_d$$

$$q_{t,r} = \int \frac{(t f_{HG} + r_1) + (t f_{HG} + r_2)}{2} \sin\cos d\theta$$

$$q_{d,t} = \int (\quad f_{HG})^{1/2} \sin\cos d\theta$$

$$\quad_d = \int f_d \sin d\theta = \text{constant}$$

$$q_{t,r} = \int_0^{\pi} \left(f_{HG} + \frac{r_1 + r_2}{2}\right)\sin\theta\, d\theta = \text{constant}$$

$$q_{d,t} = \int_0^{\pi} (f_d\, f_{HG})^{1/2} \sin\theta\, d\theta \qquad (23)$$

so that the asymmetry factor, G, of our artificial phase function, measured or determined by the Mie theory, will be:

$$G = \frac{\gamma g_d + (1-\gamma)\, g_{t,r} + 2\cos\varphi_0 \sqrt{\gamma(1-\gamma)}\, g_{d,t}}{\gamma q_d + (1-\gamma)\, q_{t,r} + 2\cos\varphi_0 \sqrt{\gamma(1-\gamma)}\, q_{d,t}} \qquad (24)$$

that is, γ is uniquely determined as the solution of a rational equation of the kind:

$$a\gamma + b\sqrt{\gamma(\gamma-1)} + c = 0 \qquad (25)$$

where a, b and c are:

$$a = q_d - q_{t,r} + 2G(r + t - 1)$$
$$b = 2\cos\varphi_0 (q_{d,t} - [illegible]\, q_{d,t}) \qquad (26)$$
$$c = q_{t,r} - 2G(r + t)$$

In summary, if all the approximations made are reasonable, and this has still to be proven, we have constructed a phase function that is able to simulate the measured phase function for a convenient choice of the free parameter γ, and for given values of the size parameter x_d, the multiplying factors and the complex refractive index m. In addition, it is possible to predict phase functions of particles with similar shape (same value of γ) for all the other

values of x (and eventually m) where the Mie theory is not a better approximation.

Figures 10 and 11 show examples of the comparison between the experimental data and the simulated phase function as obtained from Eqs. 24 and 18. Fig. 10 is for sodium chloride; γ is equal to 1.6 and g = 0.4. Fig. 11 is for methylene blue; γ is equal to 1.0 and G to 0.8. These fits are similar to those already discussed in the previous section with the same disagreement at backward scattering angles. In fact, this second formulation did not change anything in that portion of the phase function. Table II lists the values assumed by χ^2 for the sodium chloride aerosols of Fig. 10; here χ^2 is defined as:

$$\chi^2 = \sum_i \sum_j \left(1 - \frac{p_i(\theta_j)}{\tilde{p}_i(\theta_j)}\right)^2 \qquad (27)$$

where $\tilde{p}_i(\theta_j)$ are the values of the semi-empirical phase functions.

We can conclude that the assumptions made in determining Eq. 18 approximate the scattering processes in the cases analyzed, and that with the use of Fig. 7b, we can similarly reconstruct other phase functions.

As a final comment, we observe that if the equations would be precise, the quantity γ should be constant and identically equal to 0.5. Therefore, the fluctuations of γ around the value of 0.5 in Table II are a quantitative estimate of the goodness of the approximations.

6. CONCLUSIONS

Schuerman et al., through the study of different classes of well-defined geometries, presented precisely measured phase functions in each case. Coletti and Grams (1982) observed that the phase functions of particles of sodium chloride similar but not identical to each other, were indistinguishable from the phase functions of particles of ammonium sulfate crystallizing with completely different shape, analogous size and similar refractive index. That is, the slight geometrical differences occuring between particles of the same salt, are enough to wash out, in the scattering phase function, the characteristics related to a specific shape. This observation gave a more general meaning, from the application point of view, to these measurements, even though they were affected by larger experimental uncertainties.

The fitting procedure described in this article is a mathematical representation of the intuitively simple physical concepts of diffraction, reflection, and refraction. When combined, these concepts describe the light scattering observed experimentally with only small uncertainties. The experimental results of Figs. 7 and 8 showing analogies between the measured value of asymmetry factors and those computed with the Mie theory have demonstrated that applying the laws of geometric optics to monodisperse aerosols, we have to disregard the law that the cross section of a particle has to be equal to twice its cross section. We could not invoke (as did Hodkinson and Greenslaves[3] and Pollack and Cuzzi[4]) any wash out effect due to size distribution (Kerker[14]), but at the same time, we were allowed to use the Mie theory for spherical particles as a suitable criterion to evaluate the interferences between the light diffracted and transmitted by the

particles.

The advantage of our empirical approach lies in the fact that with Eq. 15 and Fig. 3, we had been able to predict the set of measured phase functions. The only free empirical parameter introduced in Eq. 15 is the asymmetry factor for the transmitted component g, which depends weakly on the shape of the particles so that it can be assumed the same for different kinds of geometries. The parameters r, t and r are determined by the complex refractive index of the material and its distribution inside the particle; G (or γ) can be determined experimentally as in our cases, or calculated using Mie theory.

Table I.

Sodium Chloride

Run N	X_{SEM}		X_c	X_{Mie}	G'	G	g	c_a	c_t	c_r
62	6.68	7.3	5	5	.690	.714	.35	.565	.423	.012
16	5.2	10.4	7.8	7.8	.542	.608	.40	.332	.554	.114
15	7.8	11.4	11.4	---	.356	.485	.40	.319	.400	.281
11	10.6	13.1	12.6	---	.361	.526	.42	.360	.450	.189
81	13.6	15.0	13.1	---	.447	.594	.42	.277	.537	.187
72	23.3	24.6	22.6	---	.384	.723	.40	.422	.466	.112
2	21.9	24.0	22.8	---	.316	.669	.40	.593	.321	.086
10	25.8	29.5	27	---	.379	.702	.42	.452	.393	.155

Table II.

Values of γ and χ^2 as defined in Eq. 18 and 24 for Sodium Chloride

X_c	γ	χ^2
5.0	0.525	38.0
7.8	0.517	39.3
11.4	0.514	41.3
12.6	0.508	42.9
13.1	0.507	43.0
22.6	0.5[illegible]	50.9
22.8	0.512	51.1
27.6	0.527	48.0

REFERENCES

1. M. Rowan-Robinson, Far Infrared Astronomy, (Pergamon Press, 1976) pp. 281-283.

2. M. D. Baker and A. Coletti, Appl. Opt., 21, 2244-2252 (in press) 1982.

3. R. H. Zerull, Beitr. Phys. Atmos., 49, pp. 169-188 (1976).

4. D. W. Schuerman, R. T. Wang, B. A. Gustafson, and R. W. Schafer, Appl. Opt., 20, pp. 4043-4050 (1981).

5. R. S. Powell, R. R. Circle, D. C. Vogel, P. D. Woodson, III, and B. Donn, Planet Sci., 15, p. 1641 (1967).

6. A. C. Holland and G. Gagne, Appl. Opt., 9, p. 1113 (1970).

7. D. H. Napper and R. H. Ottewill, in Proceedings of the Interdisciplinary Conferences, M. Kerker, Ed., Clarkson College of Technology, Pottsdam, New York (1962).

8. D. A. Cross and P. Latimer, Appl. Opt., 11, p. 1125 (1972).

9. R. G. Pinnick, D. E. Carroll, and D. J. Hoffman, Appl. Opt., 15, p. 384-393 (1976).

10. J. B. Pollack, and J. N. Cuzzi, J. Atmos. Sci., 37, pp. 868-881 (1980).

11. A. Coletti and K. W. Grams, Proceedings of the XI International Laser Radar Conference, June 21-25, 1982.

12. [illegible] H. Liu, P. K. Berglund, and J. K. Agarwal, Atmos. Env., 8, pp. 717-[illegible] (1974).

13. [illegible] W. Grams, A. J. Pascher, and C. M. Wyman, Optical Eng., 14, pp. 85-90 (1975).

14. G. W. Grams, in Light Scattering by Irregularly Shaped Particles, D. W. Schuerman, Ed., pp. 243-246, Plenum, N.Y. (1980).

15. H. C. Van de Hulst, Multiple Light Scattering, Academic Press (1980).

16. M. Born and E. Wolf, Principles of Optics, Pergamon Press, (1965).

17. J. E. Hansen and L. D. Travis, Space Sci. Rev., 16, pp. 527-610 (1974).

18. J. F. Hodkinson and I. Greenleaves, J. Opt. Soc. Amer., 53, pp. 557-588 (1963).

REFERENCES

20. M. Kerker, The Scattering of Light and Other Electromagnetic Radiation, Academic Press, N.Y. (1969).

21. L. G. Henyey and I. L. Greenstein, Appl. Opt., 93, 70 (1941).

22. C. W. Berry, J. Opt. Soc. Amer., 52, pp. 888-895 (1962).

23. T. D. Proctor and C. W. Harris, Aerosol Sci., 5, pp. 81-90 (1974).

24. S. Mukai, and T. Mukai, in Light Scattering by Irregularly Shaped Particles, W. Schuermann, Ed., pp. 219-225, Plenum, N.Y. (1980).

25. H. C. Van de Hulst, Light Scattering by Small Particles, John Wiley, Inc. (1957).

26. W. Wiscombe and A. Mugnai, in Light Scattering by Irregularly Shaped Particles, W. Schuermann, Ed., pp. 141-52, Plenum, N.Y. (1980).

ACKNOWLEDGEMENTS

The author is grateful to Prof. G. W. Grams and to Prof. G. Fiocco of the Istituto di Fisica dell'Universita di Roma, for useful suggestions and generous experimental and financial support while the work was geing carried out. He wants to thank Mr. C. Wyman and Mr. C. Sciatella for useful assistance in the experimental work and all the colleagues that kindly reviewed the manuscript. The research has been supported by the U.S. Army Research Office and by the Istituto di Fisica dell'Atmosfera, Roma, (Italy).

FIGURE CAPTIONS

Fig. 1. Comparison between experimental phase function and the Mie theory for nigrosine dye crystal of about 2 μm size, on two orthogonal planes of polarization of the light. The value of g' in the insert is the non extrapolated value of the asymmetry factor. In this case, the best-fitting value of x_{Mie} is 9.4 and the complex refractive index, m, has been chosen equal to 1.67 - i0.6; the extrapolated asymmetry factor (g) is 0.884.

Fig. 2. Measured phase function for sodium chloride crystals with size about 2.8 μm (shown in the insert). The dashed line is the Fraunhofer diffraction curve for x_d = 13.1.

Fig. 3. Measured phase function for methylene blue crystals with size about 2 μm, (shown in the insert). The dashed line is the Fraunhofer diffraction curve for x_d = 11.

Fig. 4. Fresnel reflection as function of the scattering angle ; (a), for refractive index m = 1.54 - i0; (b), for refractive index m = 1.33 - i0.5.

Fig. 5. Comparison between the measured phase function for sodium chloride crystals with size about 2.8 μm and the best-fit for x_d = 13.1.

Fig. 6. Comparison between the measured phase function for methylene blue crystals of about 2 μm size and the best-fit for x_d = 11.

FIGURE CAPTIONS

(continued)

Fig. 7. (a) Contributions due to diffraction in the case of NaCl aerosol as function of the size parameter and in the approximation of negligible contributions of reflected light.

(b) Experimental values of asymmetry factor for NaCl as function of the size parameter x_d (squares) and Mie theory asymmetry factor curve for $x_{Mie} \triangleq x_d$ (continuous line); the dashed line is the Mie theory asymmetry factor curve but for $x_d \triangleq x_{Mie}$ 1.6.

Fig. 8. Root mean square deviations between experimental and Mie theory asymmetry factors as functions of the multiplying factor ζ:

(a) for NaCl

(b) for ammonium sulfate

(c) for potassium chlorate

Fig. 9. (a) Comparison for nigrosine dye between measured asymmetry factor (squares) and Mie theory curve.

(b) Root mean square deviations between Mie theory and experimental value of the asymmetry factor as function of the multiplying factor $\zeta = x_d/x_{Mie}$.

Fig. 10. Comparison between the phase functions as predicted by the semiempirical theory (for $q = 0.6$ and $\zeta = 1.6$) and the results of the experiments for sodium chloride:

(a) for $x_d = 5$.

(b) for $x_d = 7.8$.

(c) for $x_d = 11.4$.

(d) for $x_d = 22.8$.

Fig. 11. Comparison between phase function predicted by the semiempirical theory (for $q = 0.6$ and $\zeta = 1$) and the results of the experiments for methylene blue with size parameter $x_d = 11$.

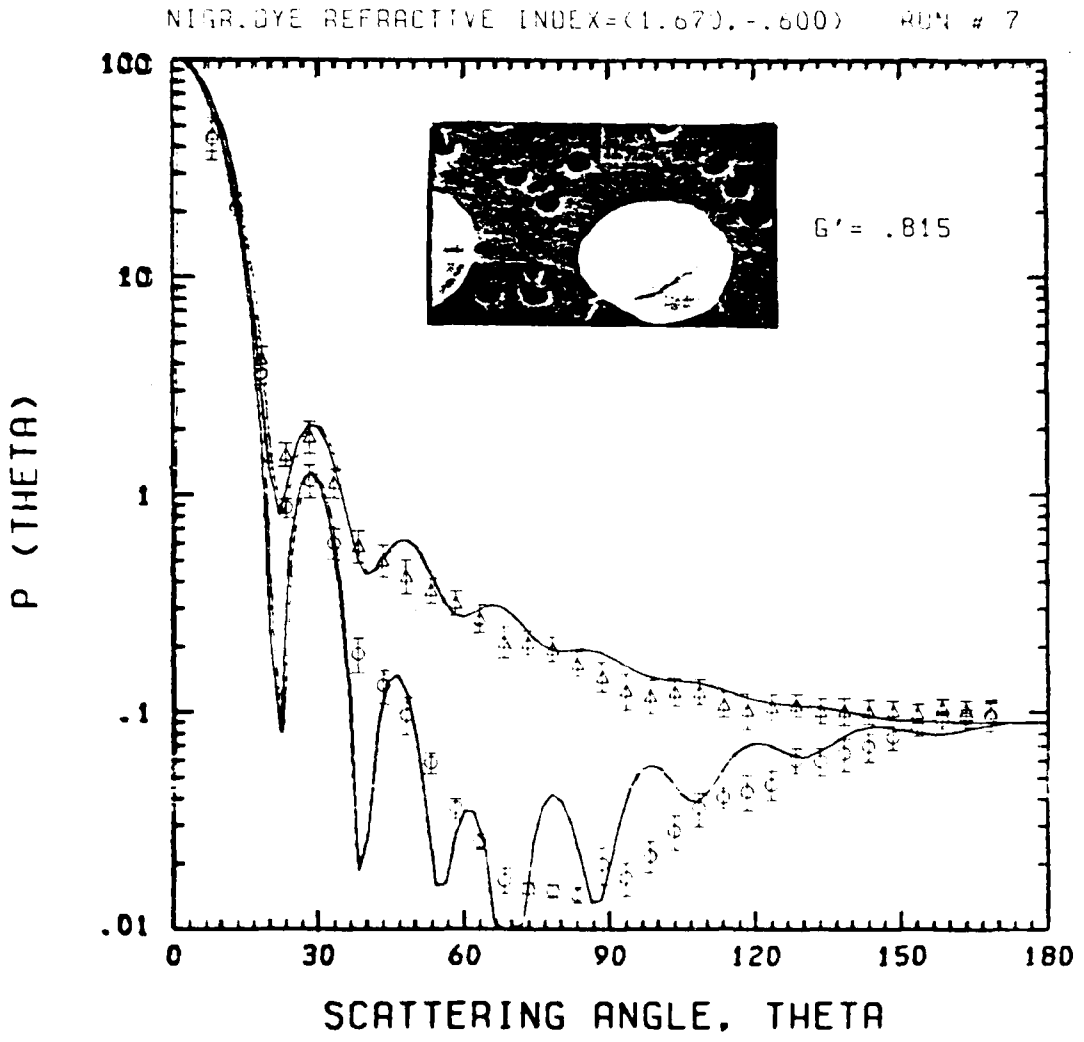

X = 9.4
G = .884

Figure 1.

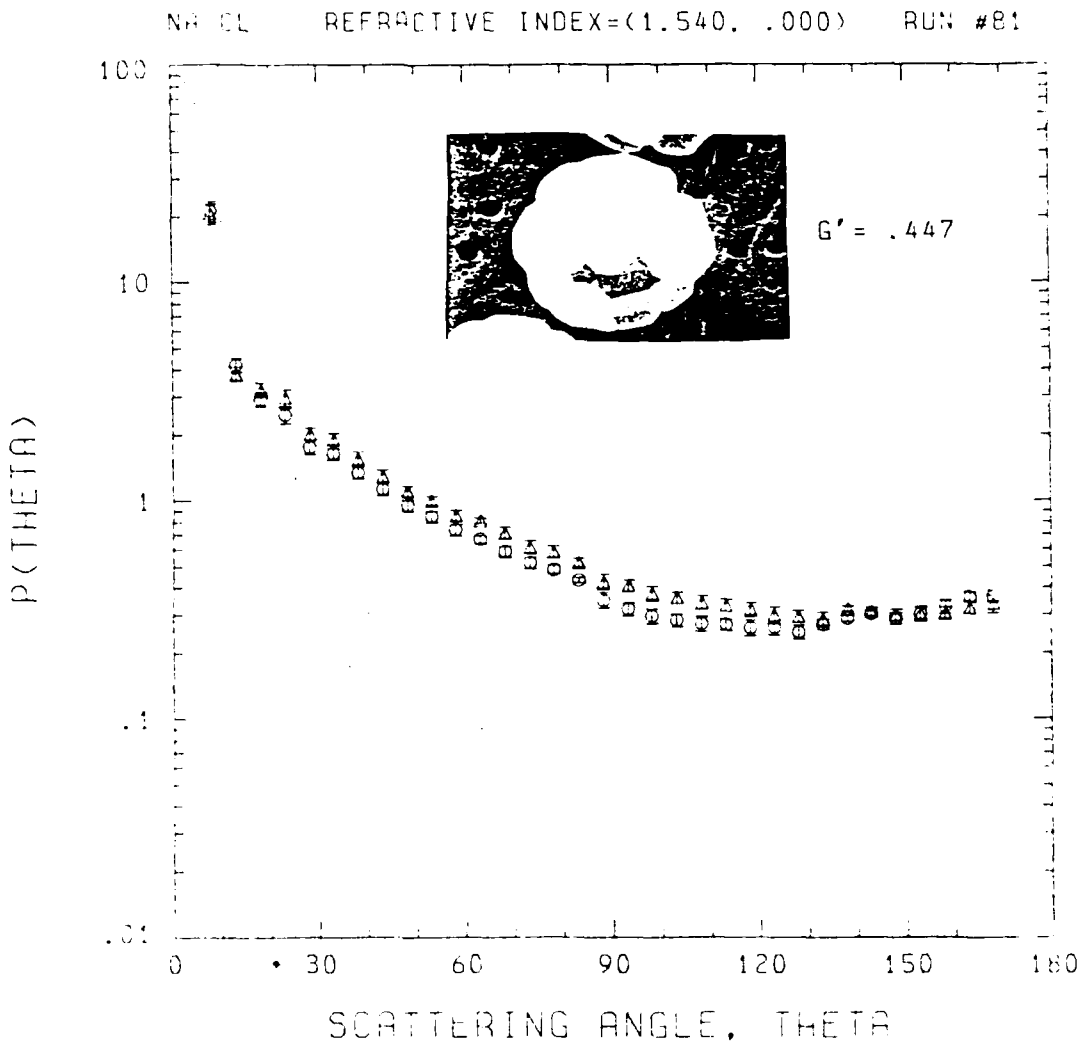

X = 13.1
G = .594

Figure 2.

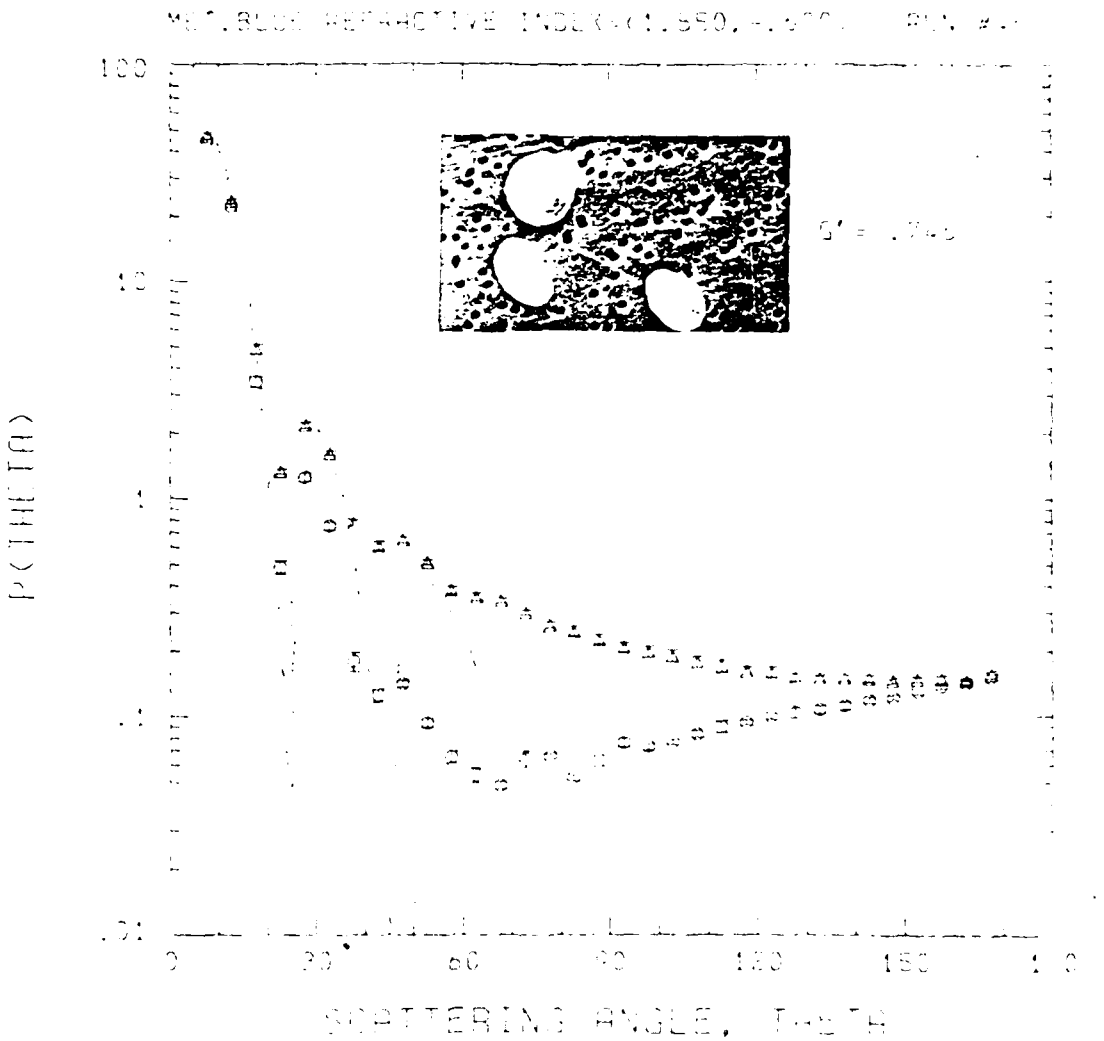
P(THETA)
100
10
1
.1
.01
0
30
60
90
120
150
180
SCATTERING ANGLE, THETA
X = 11.0
G = .820

Figure 3.

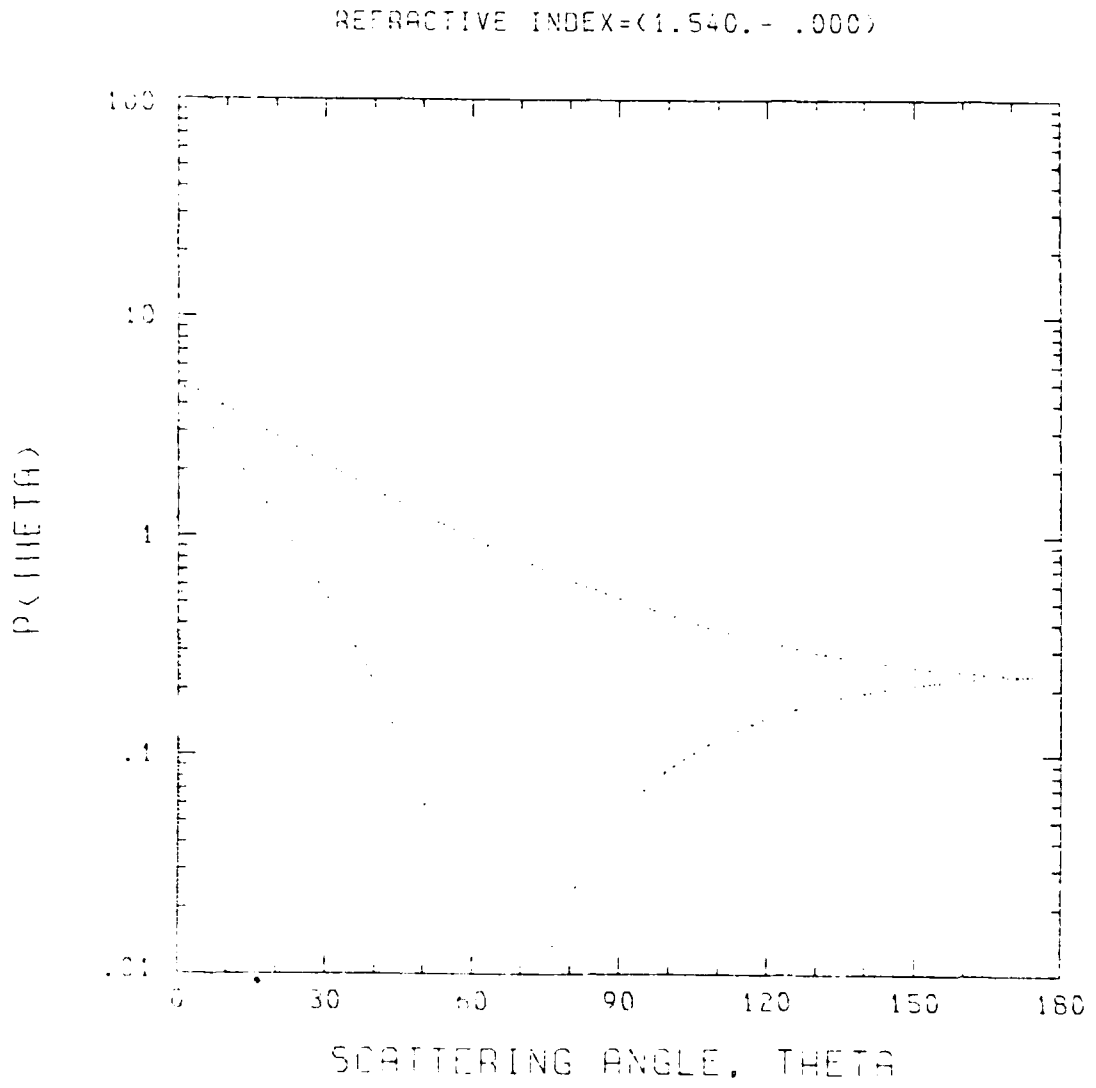
REFRACTIVE INDEX=(1.540,- .000)
100
10
1
.1
.01
P(THETA)
0
30
60
90
120
150
180
SCATTERING ANGLE, THETA

Figure 4a.

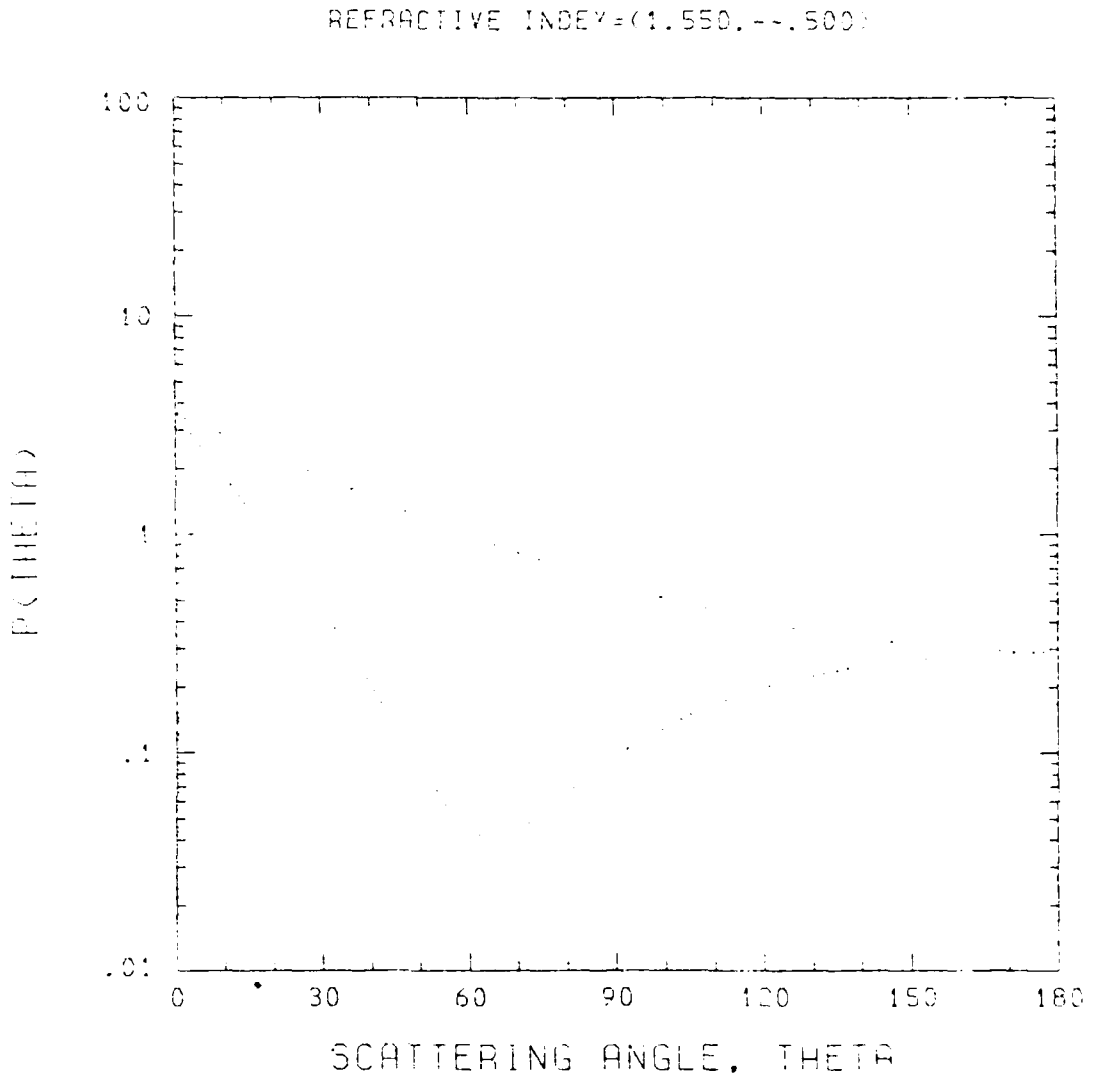
REFRACTIVE INDEX=(1.550,-.500)
100
10
1
.1
.01
0
30
60
90
120
150
180
SCATTERING ANGLE, THETA

Figure 4b.

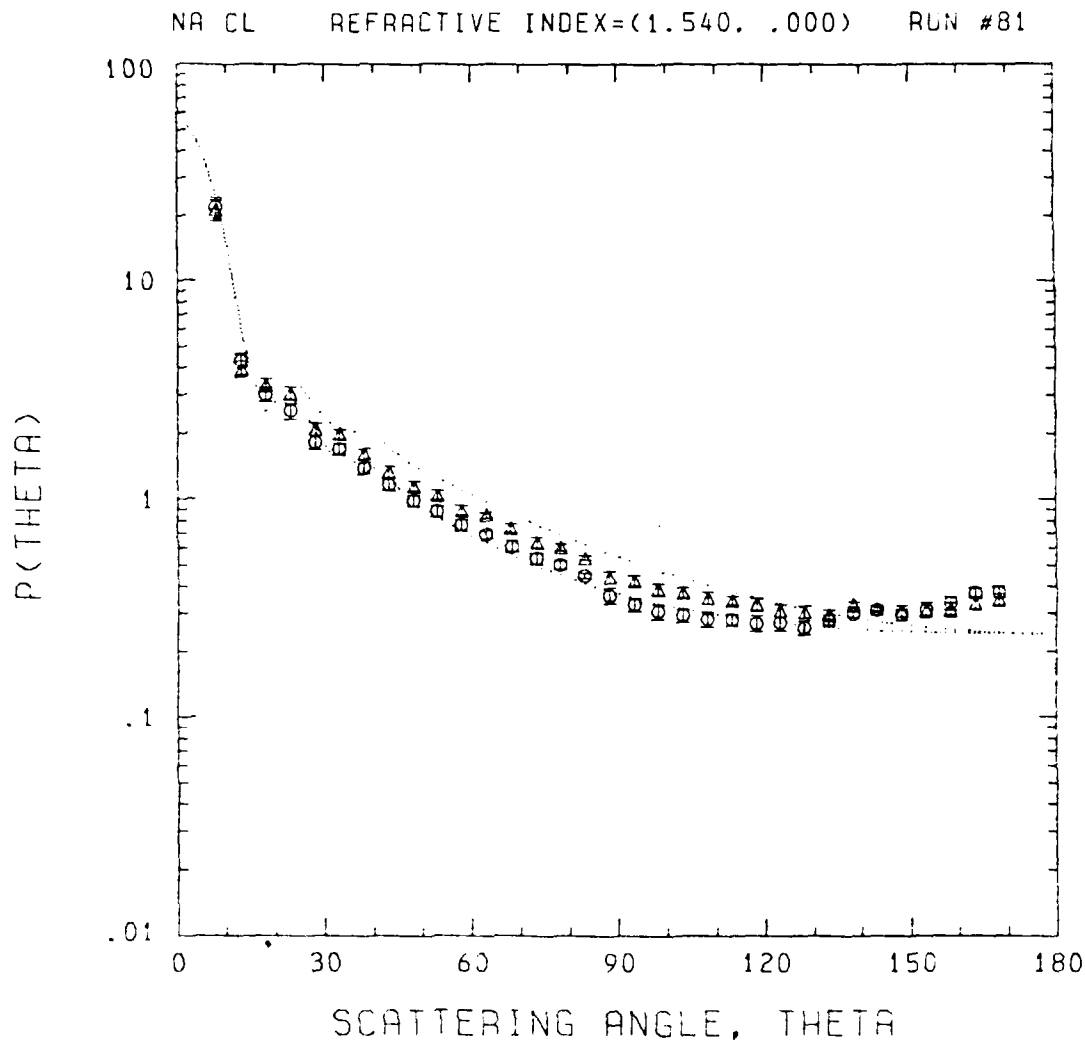

X = 13.1
g = .420

C_d .277
C_t = .537
C_r = .187

Figure 5.

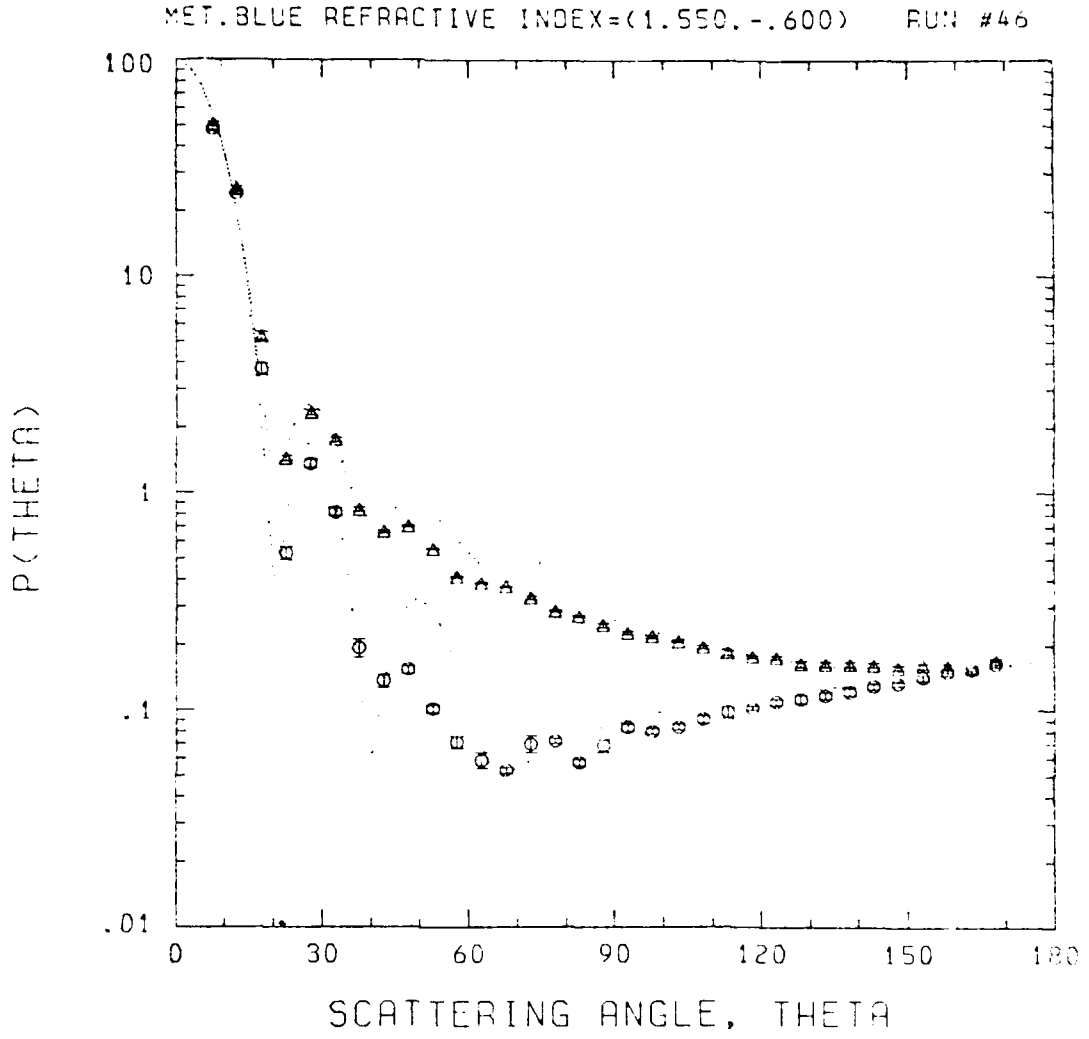

X = 11.0
g = .600

C_d = .747
C_t = .004
C_r = .249

Figure 6.

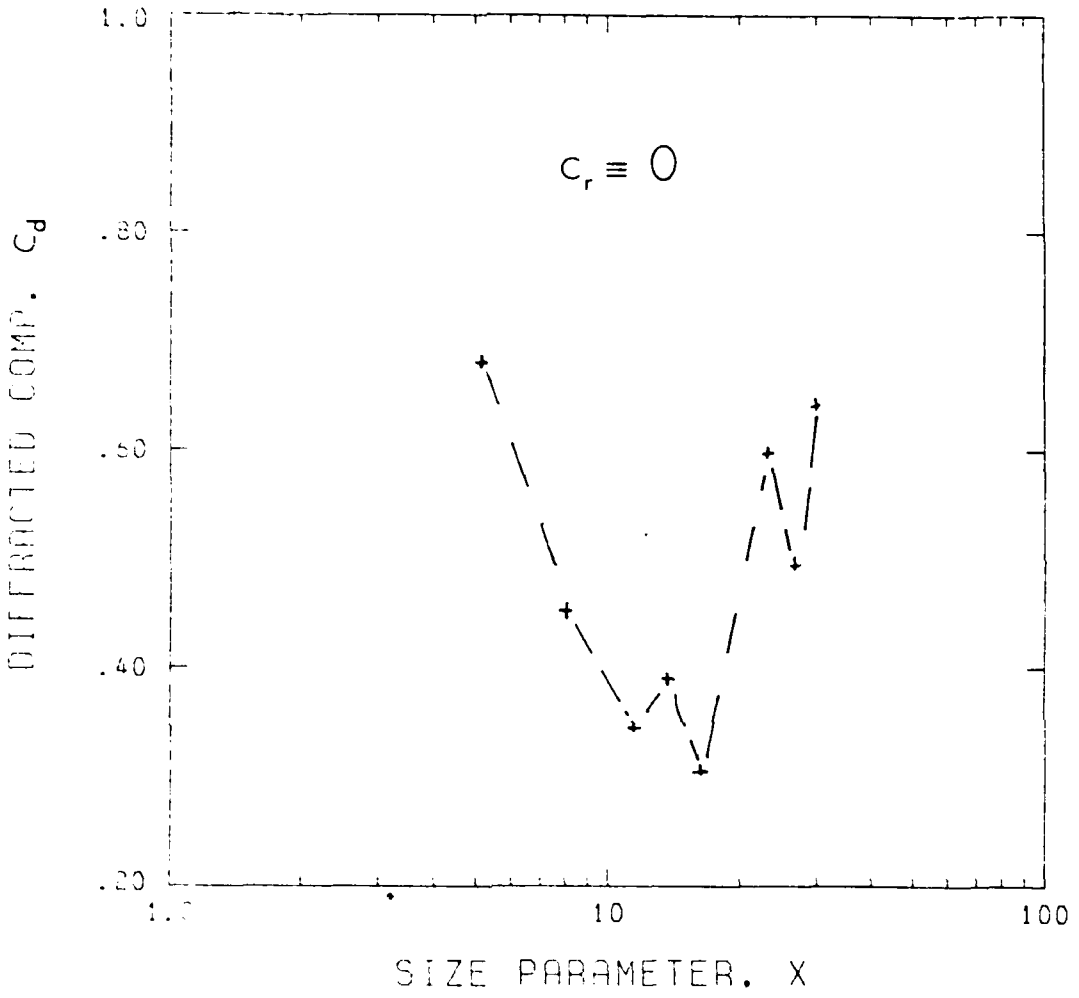
1.0
.80
.60
.40
.20
$C_r \equiv 0$
DIFFRACTED COMP. C_d
TRANSMITTED COMP. C_t
1.0
10
100
SIZE PARAMETER, X

Figure 7a.

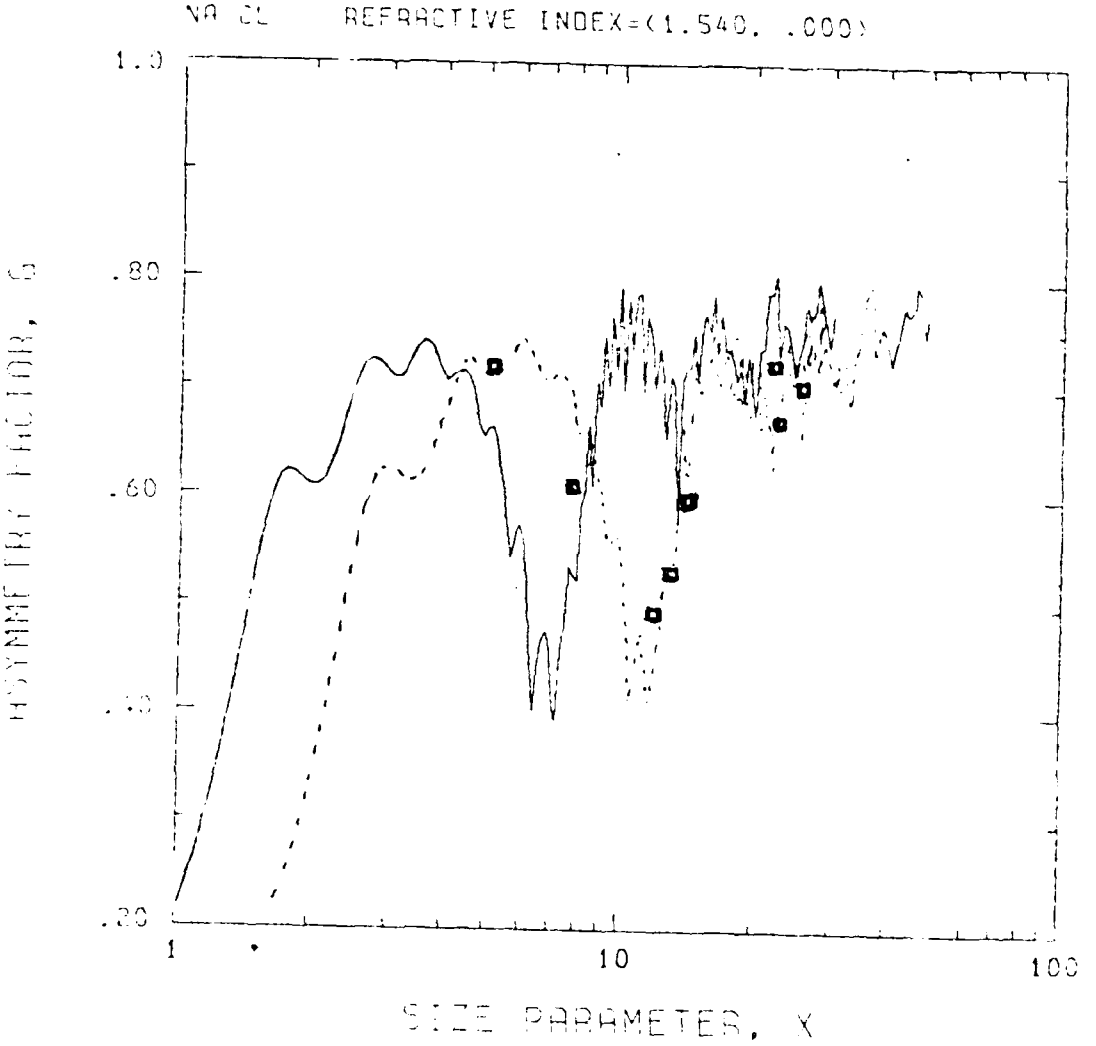
NA CL REFRACTIVE INDEX=(1.540, .000)
1.0
.80
.60
.20
1
10
100
SIZE PARAMETER, X

Figure 7b.

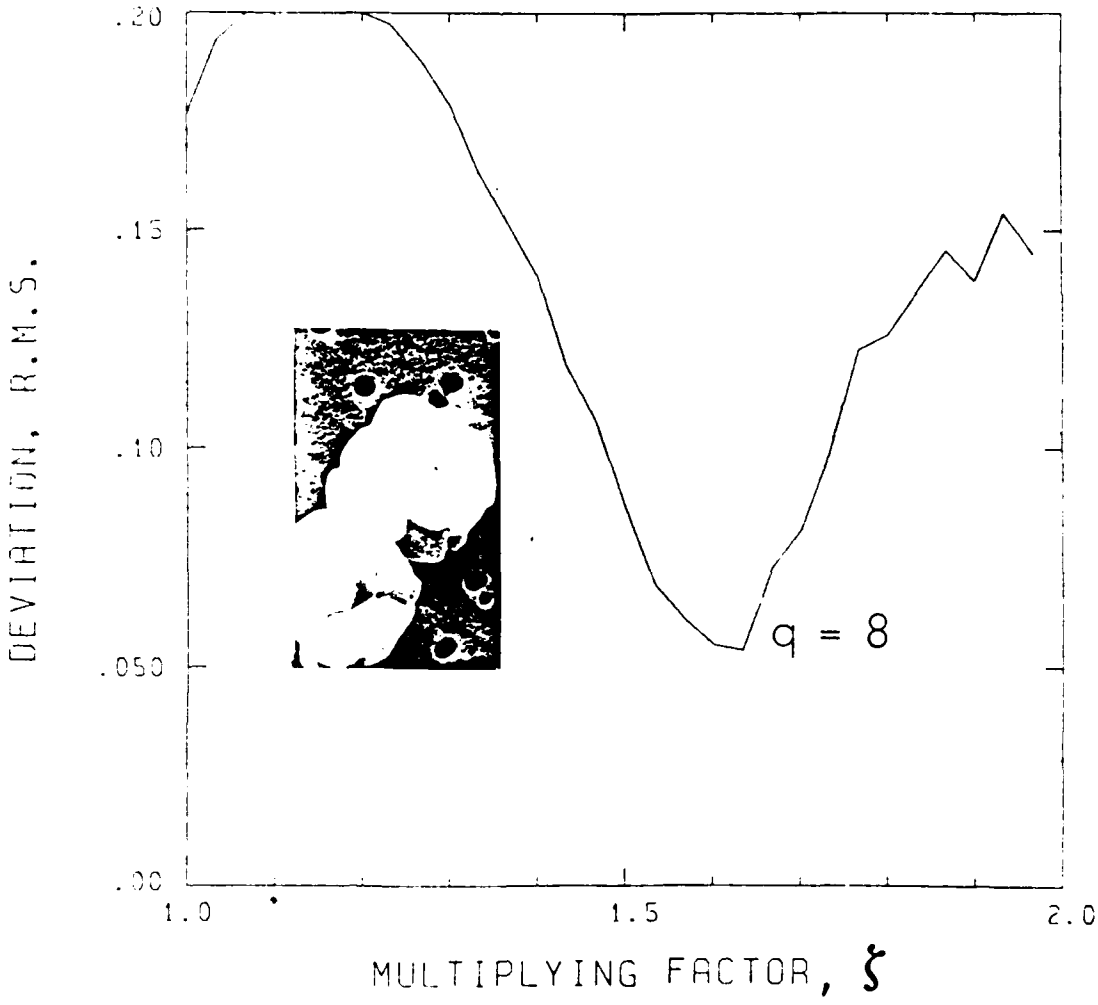

Figure 8a.

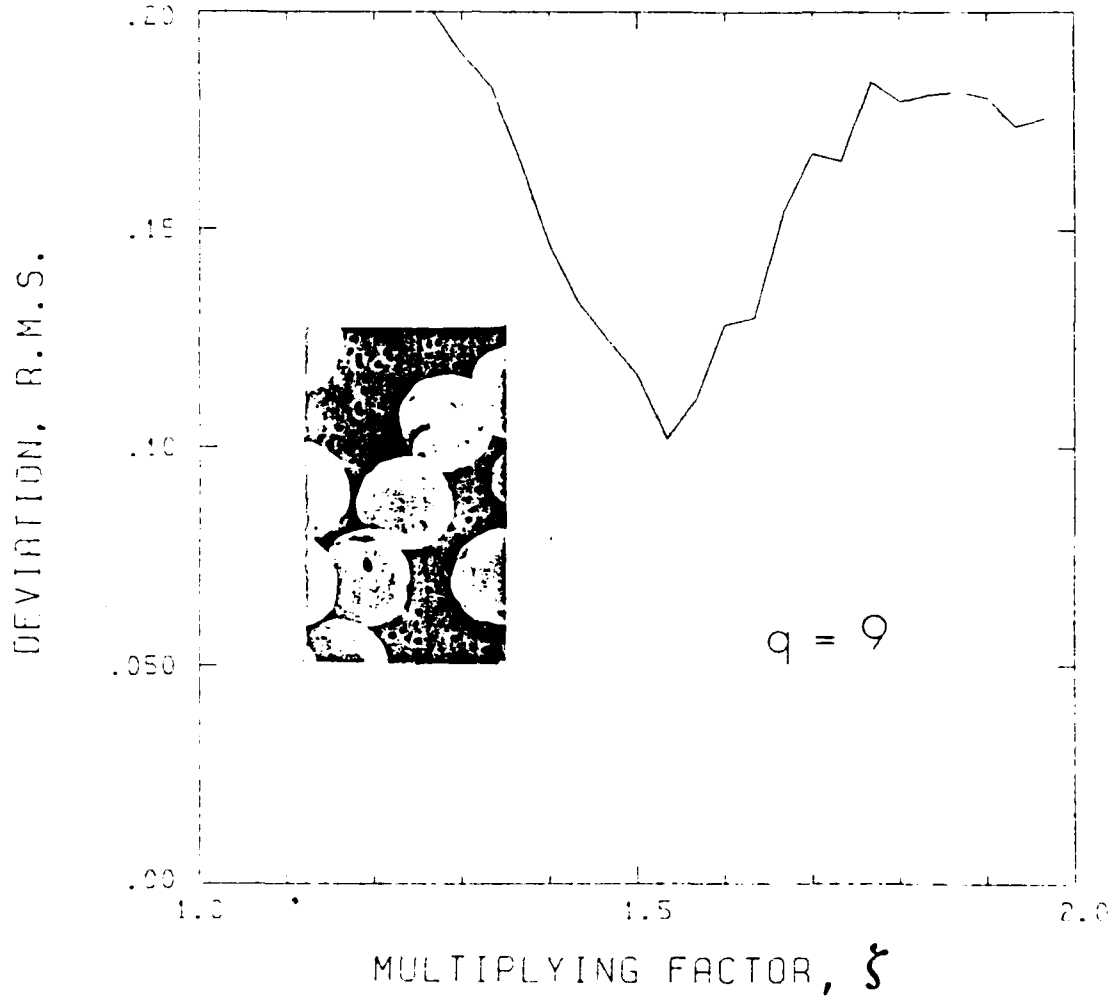

Figure 8b.

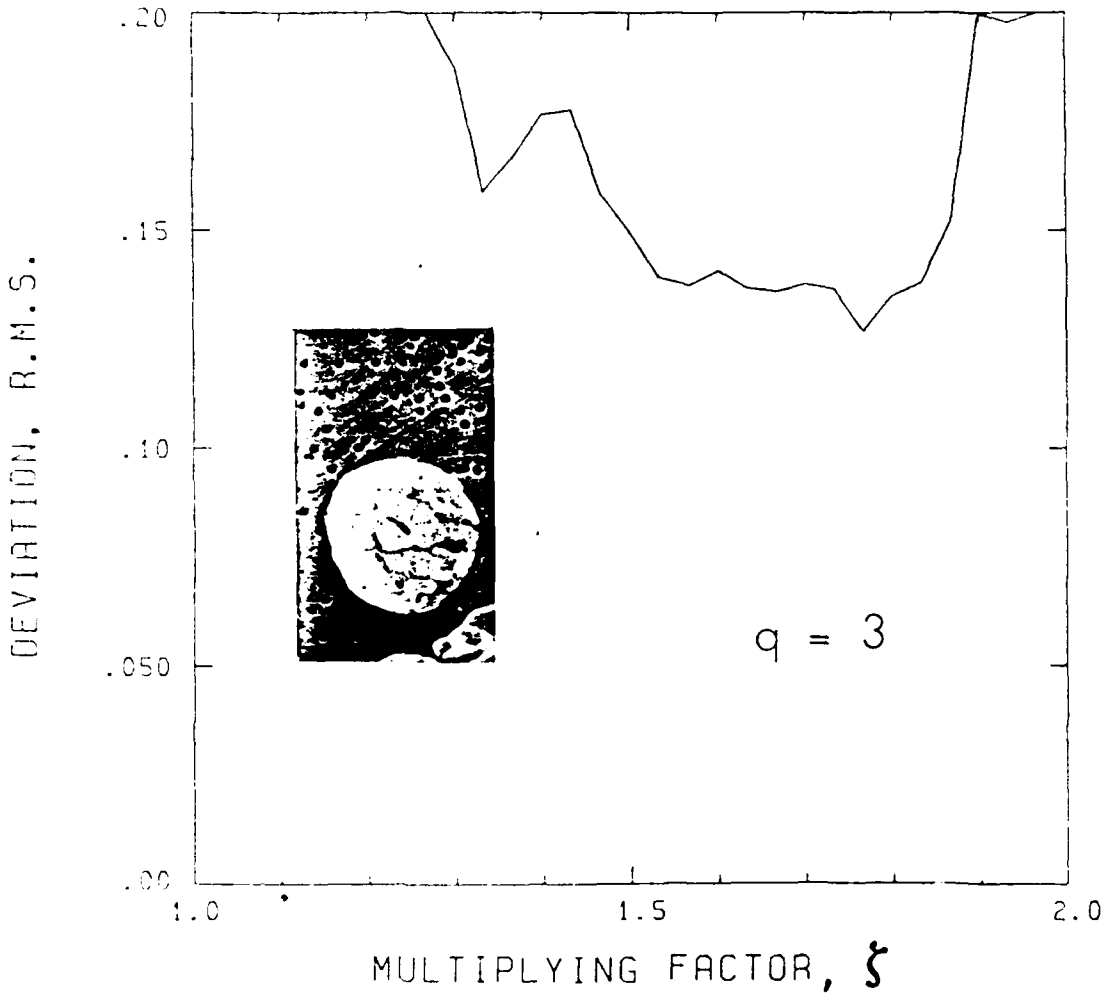

Figure 8c.

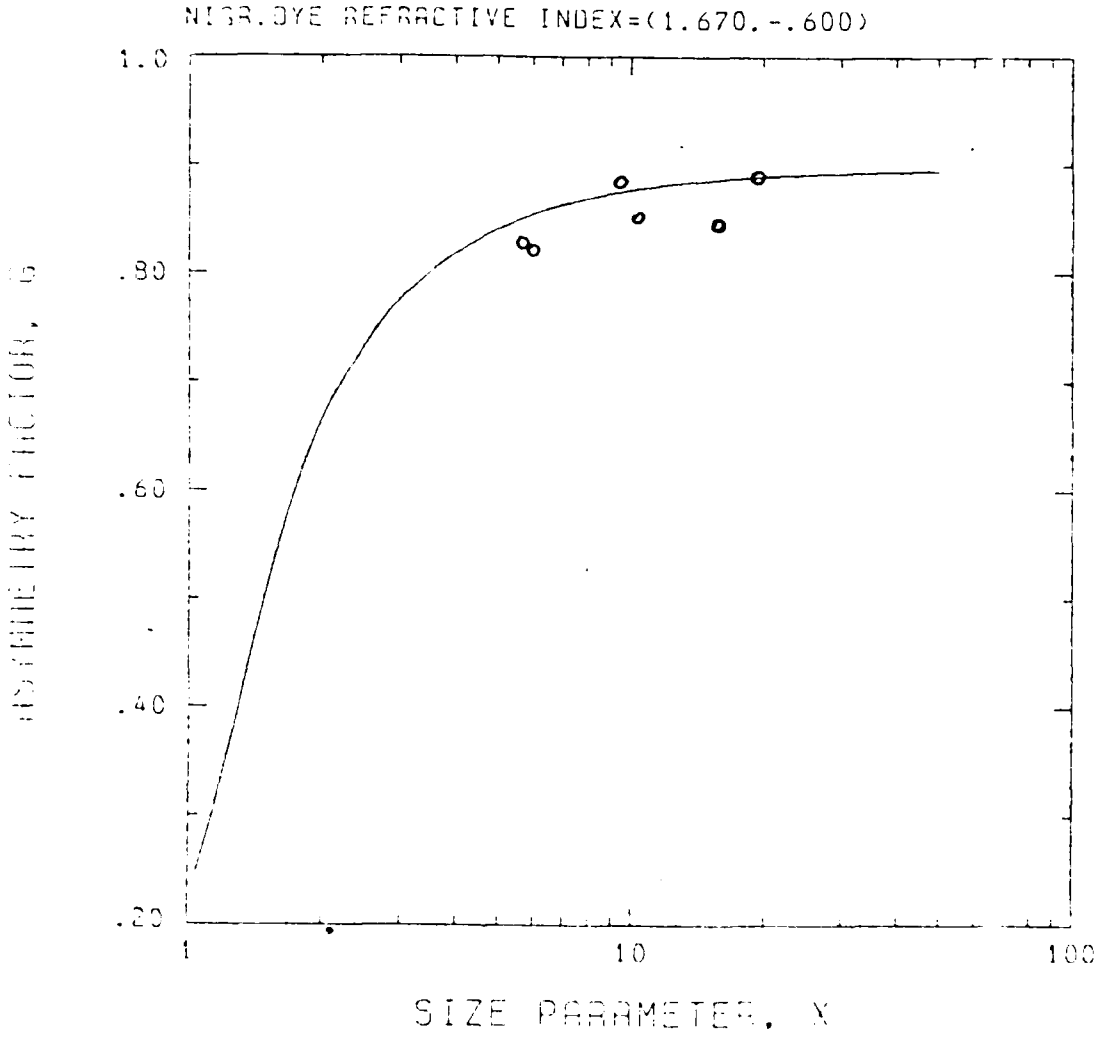
NIGR.DYE REFRACTIVE INDEX=(1.670,-.600)
1.0
.80
.60
.40
.20
1
10
100
SIZE PARAMETER, X

Figure 9a.

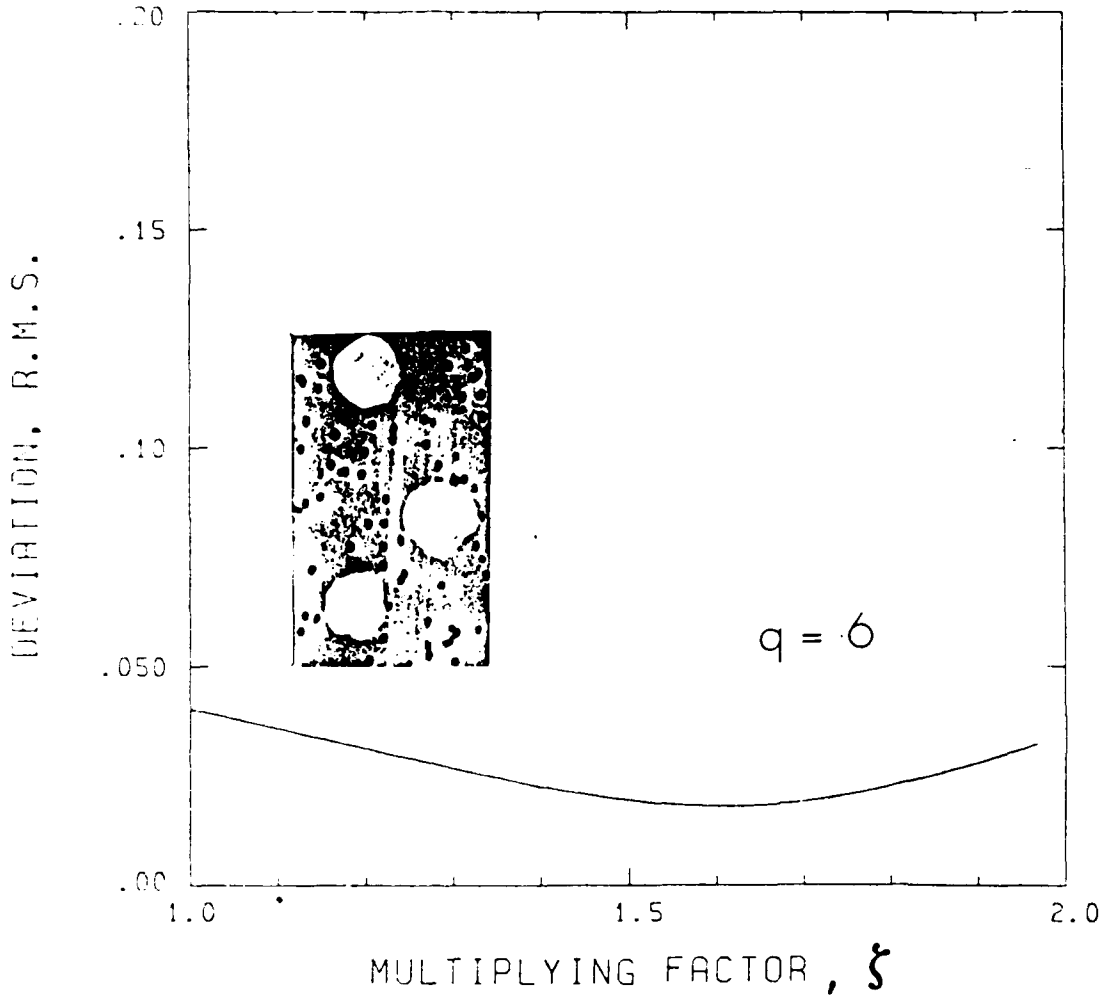

Figure 9b.

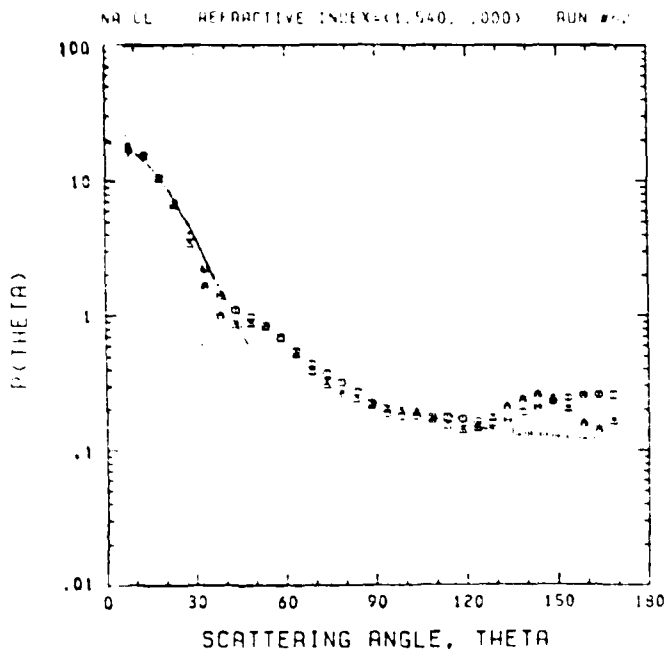

x = 5.0 (a)

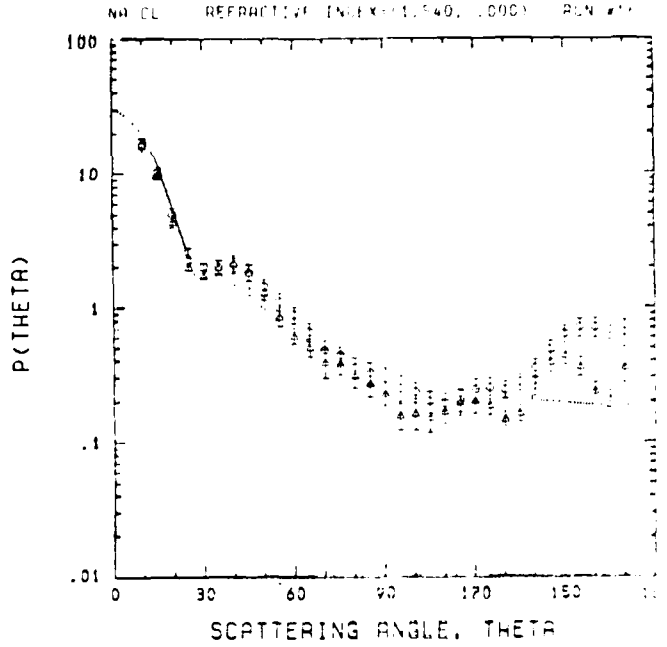

x = 7.8 (b)

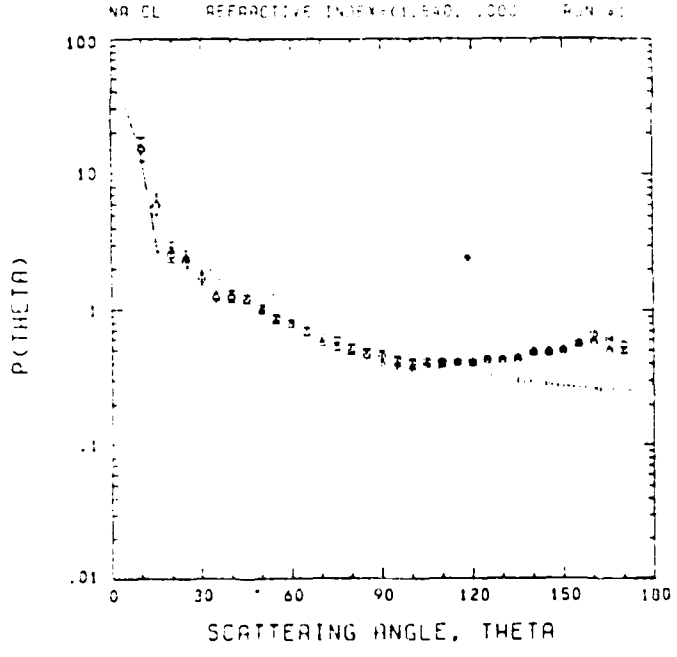

x = 11.4 (c)

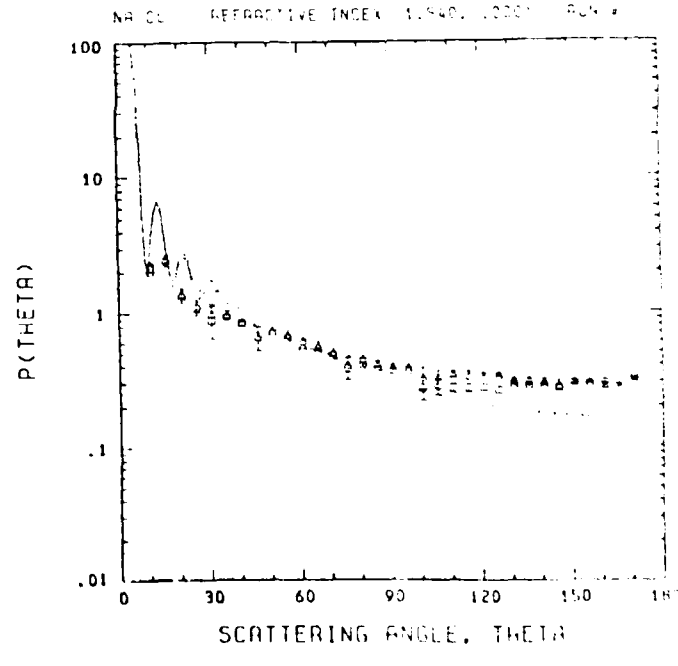

x = 22.8 (d)

Figure 10.

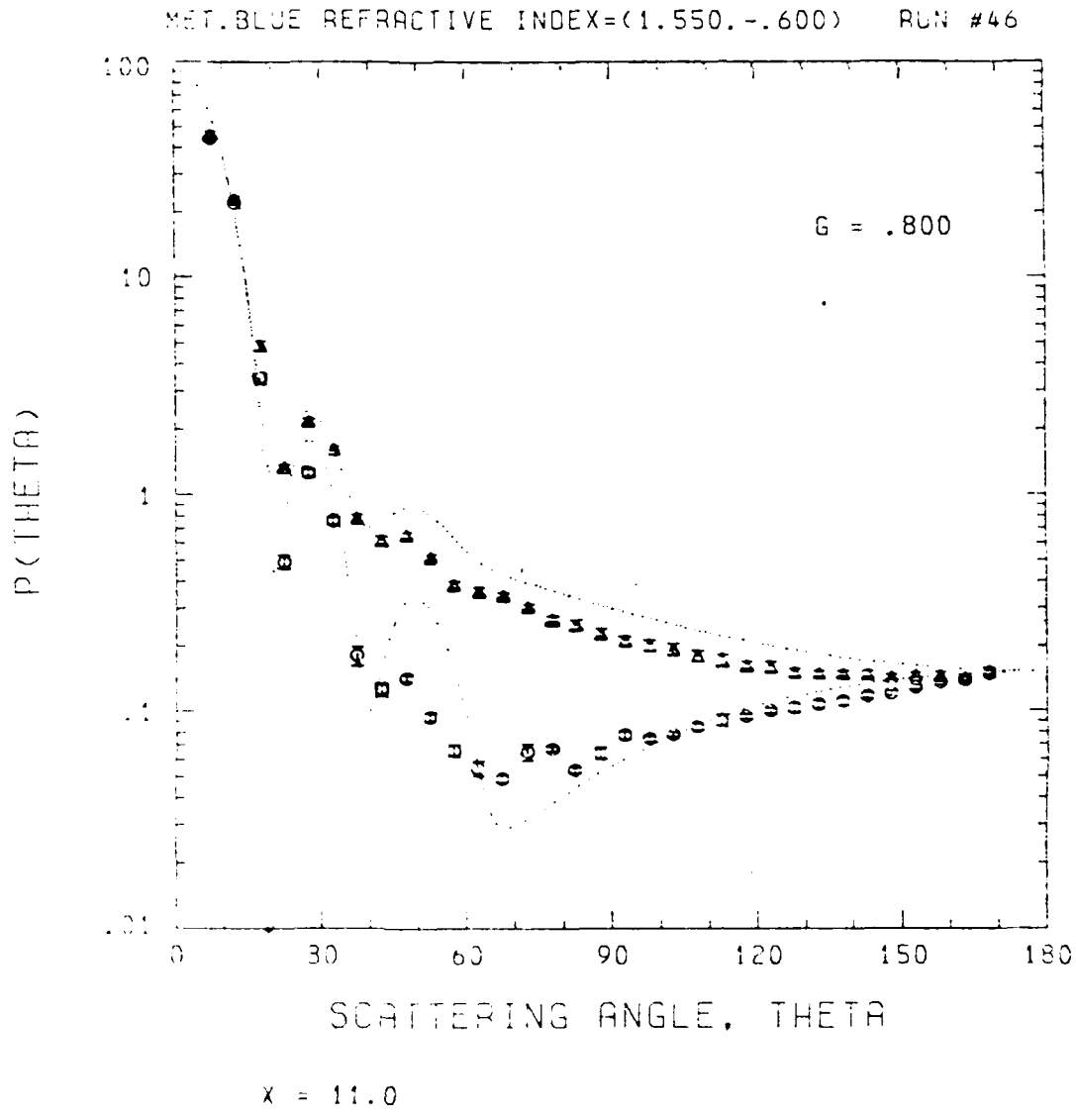
MET.BLUE REFRACTIVE INDEX=(1.550,-.600) RUN #46
100
10
1
.1
.01
P(THETA)
G = .800
0
30
60
90
120
150
180
SCATTERING ANGLE, THETA
X = 11.0

Figure 11.


DAT
FILM